MAX PLANCK INSTITUTE FOR BIOGEOCHEMISTRY

Abschlussbericht

Eingehende Darstellung

Das Potential von Erdbeobachtungen zur Erfassung von Mustern der Biodiversität Europäischer Wälder und Analyse deren Resilienz.

The Potential of Earth Observations to Capture Patterns of Biodiversity

OBEF-Accross2

Dr. Javier Pacheco-Labrador (https://orcid.org/0000-0003-3401-7081)
Dr. Mirco Migliavacca (https://orcid.org/0000-0003-3546-8407)
Xuanlong Ma (https://orcid.org/0000-0003-3263-0616)
Miguel Machecha (https://orcid.org/0000-0003-3031-613X)
12/31/2022

Förderkennzeichen: 50EE1912

Projektleitung:Herr Dr. Pacheco-Labrador

Contents

Contents 1

Abschnitt 1. Kurzdarstellung (Short summary) 3

Abschnitt 2. Eingehende Darstellung (In-depth technical report in the English language) 6

TASK 1. TO DEVELOP A METHOD TO INTEGRATE SATELLITE DATA STREAMS FROM MULTIPLE SOURCES (MULTI-SPECTRAL, HYPERSPECTRAL, RADAR) TO PREDICT BOTH TAXONOMIC DIVERSITY (TD) AND FUNCTIONAL DIVERSITY (FD). 6

TASK 2. MAPPING OF TD AND FD IN EUROPEAN FOREST ECOSYSTEMS USING THE METHODS DEVELOPED IN RESEARCH OBJECTIVE 1. 45

TASK 3. TO ANALYSE THE IMPACT OF BIODIVERSITY ON ECOSYSTEM FUNCTIONS AND THEIR RESILIENCE. 50

REFERENCES 56

Im folgenden Zwischenbericht stellen wir die im ersten Jahr der Aktivitäten im Rahmen des Projekts Nr. 50EE1621 erzielten Ergebnisse vor. Der erste Teil ist eine Zusammenfassung (in deutscher und englischer Sprache). Der zweite Teil des Berichts (in englischer Sprache) ist die ausführliche technische Beschreibung der wichtigsten Ergebnisse und Erungenschaften, die während der Projektdurchführung (Jan-2021 - Dez-2022) erzielt wurden. Der Finanzbericht wurde in einem separaten Dokument versandt.

In the following intermediate report, we present the results obtained during the second year of activities in the context of project No. 50EE1912. The first part is a summary (in German and English language). The second part of the report (written in English) is the in-depth technical description of the project's most important results and achievements during the execution period Jan-2021 – Dec-2022. The financial report will be sent in a separate document.

Abschnitt 1. Kurzdarstellung (Short summary)

German Version

Der folgende Abschnitt fasst die wissenschaftlichen und technischen Leistungen und Beiträge zusammen, die während der gesamten Laufzeit von OBEF-Accross2 erbracht wurden. Wir haben die meisten der geplanten Ziele erfolgreich erreicht und unerwartete und sehr wichtige Beiträge geleistet. Darüber hinaus haben wir die Projekterwartungen in Bezug auf die methodische Entwicklung und Bewertung übertroffen. Diese Erfolge lassen sich wie folgt zusammenfassen:

1) Wir haben robuste Simulationsrahmen entwickelt, die es uns ermöglichten, mehrere methodische Ansätze für die Fernschätzung der funktionalen Vielfalt von Pflanzen auf verschiedenen Ebenen zu bewerten. Die Plausibilität der Rahmenwerke wurde anhand von Fernerkundung (RS) und Feldbeobachtungen validiert.
2) Zum ersten Mal haben wir vier relevante Fragen bezüglich des Potenzials und der Grenzen der Fernerkundung der funktionellen Vielfalt von Pflanzen auf robuste und verallgemeinerbare Weise beantwortet: 1) Welche Metriken der funktionellen Vielfalt (FDM) können die funktionelle Vielfalt von Pflanzen aus dem Weltraum erfassen? 2) Können spektrale Merkmale (z. B. Reflexionsfaktoren) oder optische Merkmale (Schätzungen von Pflanzeneigenschaften) die funktionelle Vielfalt von Pflanzen erfassen? 3) Können Einzelbildanalysen die funktionelle Vielfalt von Pflanzen auf eine Weise ableiten, die auf lokaler und globaler Ebene vergleichbar ist? und 4) Wie wirken sich die verschiedenen RS-Merkmale (d.h. spektrale Konfiguration, räumliche Auflösung und Unsicherheit) auf die Schätzung der funktionellen Vielfalt von Pflanzen aus?
3) Wir haben eine globale Normalisierungsmethode entwickelt, die direkt vergleichbare FDMs für verschiedene RS-Missionen und Felddatensätze liefert. Darüber hinaus ermöglichte der neue Ansatz zum ersten Mal die Verwendung *äquivalenter Zahlenmetriken* in der RS, die eine unvoreingenommene Partitionierung der Biodiversität auf verschiedenen Skalen (Alpha, Beta und Gamma) unter Verwendung von FDMs ermöglichen.
4) Wir haben die Rolle verschiedener Pflanzenmerkmale in den Beziehungen zwischen funktionaler und spektraler Pflanzenvielfalt mit Hilfe von Techniken des maschinellen Lernens und der Modellanalyse bewertet.
5) Wir haben weltraumgestützte Bilder von DESIS- und Sentinel-2 MSI-Sensoren verarbeitet, um Karten der funktionalen Vielfalt des FunDivEUROPE-Netzwerks zu erstellen und sie mit Felddaten zu vergleichen. Darüber hinaus haben wir die Sentinel-2-Zeitreihenanalyse erweitert, um die funktionelle Vielfalt von Pflanzen in Wirbelstrom-Kovarianz-Stationen zu kartieren, um Analysen der Biodiversität und der Ökosystemfunktionen zu unterstützen. In diesem Zusammenhang haben wir Möglichkeiten zur Verbesserung der Charakterisierung und

Interpretation der zeitlichen Variabilität der funktionellen Vielfalt von Pflanzen untersucht.

6) Wir haben eine Verarbeitungskette für die Kartierung der funktionellen Vielfalt aus Sentinel-2-Bildern konzipiert und die verbleibenden Herausforderungen für einen operationellen Aufbau identifiziert.
7) Wir haben die Beziehungen zwischen der funktionellen Vielfalt und den funktionellen Reaktionen des Ökosystems analysiert und damit die Fähigkeit der Fernerkundung zur Erklärung der funktionellen Eigenschaften von Ökosystemen und ihre zunehmende Rolle bei der Stabilität von Ökosystemen in trockenen Gebieten nachgewiesen.

English Version

The following section summarizes the scientific and technical achievements and contributions accomplished during the entire duration of OBEF-Accross2. We have successfully reached most of the scheduled objectives and goals and made unexpected and very relevant contributions. Furthermore, we exceeded project expectations in the context of methodological development and evaluation. These achievements can be summarized as follow:

1) We have developed robust simulation frameworks that allowed us to evaluate several methodological approaches for remote estimation of plant functional diversity at different scales. The frameworks' plausibility was validated using remote sensing (RS) and field observations.
2) For the first time, we have answered four relevant questions regarding the potential and limitations of remote sensing of plant functional diversity in a robust and generalizable way: 1) which functional diversity metrics (FDMs) can capture plant functional diversity from space? 2) Can spectral traits (e.g., reflectance factors) or optical traits (plant trait estimates) capture plant functional diversity? 3) Can single-image analyses infer plant functional diversity in a way comparable at local and global scales? and 4) How do the different RS features (i.e., spectral configuration, spatial resolution, and uncertainty) affect the estimation of plant functional diversity?
3) We have developed a global normalization method that provides directly comparable FDMs for different RS missions and field datasets. In addition, the new approach allowed using *equivalent number* metrics in RS for the first time, providing unbiased partitioning of biodiversity at different scales (alpha, beta, and gamma) using FDMs.
4) We have evaluated the role of different plant traits in the relationships between plant functional and spectral diversity using machine learning and model analysis techniques.
5) We have processed spaceborne imagery from DESIS and Sentinel-2 MSI sensors to generate functional diversity maps of the FunDivEUROPE network and compared them with field data. Moreover, we have extended Sentinel-2 time series analysis to map plant functional diversity in eddy-

covariance stations in support of biodiversity-ecosystem function analyses. In this context, we have explored ways to improve the characterization and interpretation of the temporal variability of plant functional diversity.

6) We have conceptualized a processing chain to map functional diversity from Sentinel-2 imagery and identified the remaining challenges to achieve an operational setup.
7) We have analyzed the relationships between functional diversity and ecosystem functional responses, proving the capability of remote sensing to explain ecosystem functional properties and its increasing role in ecosystem stability in arid environments.

Abschnitt 2. Eingehende Darstellung (In-depth technical report in the English language)

TASK 1. TO DEVELOP A METHOD TO INTEGRATE SATELLITE DATA STREAMS FROM MULTIPLE SOURCES (MULTI-SPECTRAL, HYPERSPECTRAL, RADAR) TO PREDICT BOTH TAXONOMIC DIVERSITY (TD) AND FUNCTIONAL DIVERSITY (FD).

(Vorhersage von TD und FD über die spektrale Diversität)

oBEF-Accross2 has broken methodological barriers in remote sensing (RS) of plant biodiversity. This field has rapidly developed over the last few years, pushed by the urgent need to create a global monitoring system that supports the measures against the biodiversity crisis. However, the empirical and local character of most studies limited advances in the field. The lacking overlap of ecosystems, metrics, methods and sensors used in the different analyses prevented providing robust and generalizable answers to fundamental questions regarding the potential and limitations of RS to characterize plant biodiversity from space. Whereas oBEF-Accross2 was conceived with an empirical spirit, during the project's first year (Y1), we realized that we needed a more mechanistic understanding of the spectral and plant functional diversity relationships. The most relevant contribution of oBEF-Accross2 has been adopting a new way to answer the most basic questions. Beyond the project expectations, we have developed modeling frameworks to simulate plant and spectral diversity mechanistically connected by radiative transfer theory.

This approach opened the door to answering relevant methodological questions and developing new metrics that solved some of the problems inherent to remote sensing. However, it also helped us realize that some of the foreseen observational datasets the project intended to use were suboptimal for the pursued objectives. Consequently, the unexplored potential of this tool made us dedicate more resources than expected to this Task 1, with results beyond our original expectations. Nonetheless, modeling efforts have been complemented as much as possible with observational data to test its plausibility and dutifully address all the project objectives and tasks. The overall result has been positive for the project's impact. At the present stage of development in remote sensing of plant biodiversity, answering the critical methodological questions is a fundamental and necessary step. Consequently, we expect oBEF-Accross2 results to become referential and guide future developments in the field.

While the project aimed at estimating taxonomical diversity, our results and recent literature (Fassnacht et al. 2022) suggest that remote sensing might not be a convenient tool to do this generally. Therefore, while we always checked, most project results and efforts focused on functional diversity.

RD1.1: Prediction of TD and FD over spectral diversity

This Research and Development (RD) task aimed to decypher the relationships between plant and spectral diversity, initially using observational datasets from remote sensing missions and field plots. However, early results suggested that only this information would not allow us to reveal the underlying mechanisms behind the weak relationships found, nor the role of different confounding factors (Figure 1). For this reason, oBEF-Accross2 developed radiative transfer-based simulation frameworks that solved the emerging fundamental questions.

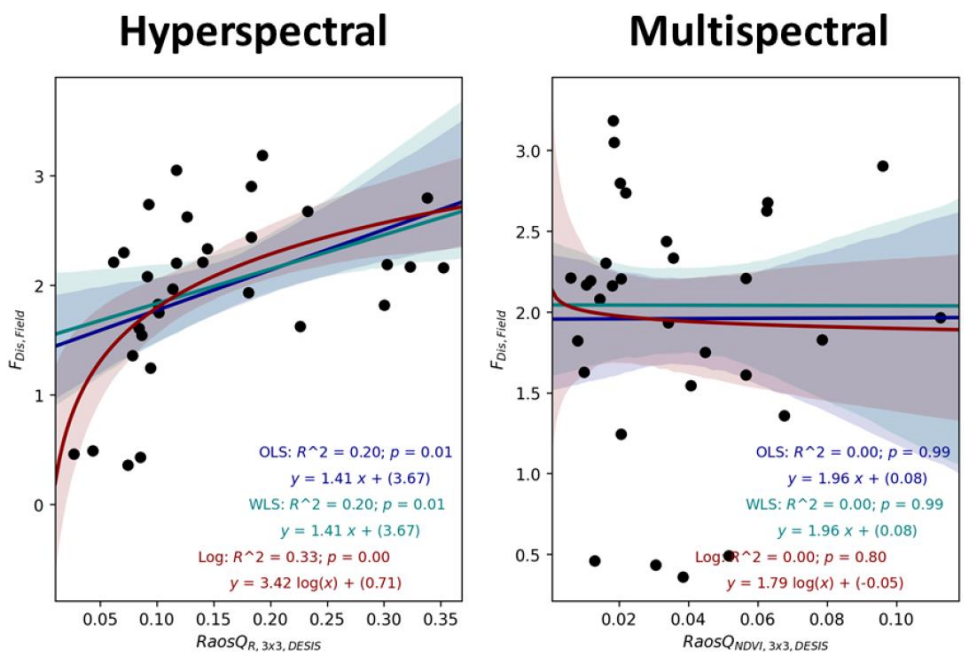

Figure 1. Comparison of field estimates of Functional Dispersion with Rao's *Q* derived from DESIS hyperspectral imagery (left) or the Normalized Difference Vegetation Index (right) in FunDivEUROPE sites.

RD1.1.a. Development of simulation frameworks for spectral and functional diversity analysis

We developed a simulation framework during the project's first year (Y1), which was consolidated during the second year (Y2). However, we found that such a simulation framework is not a tool for every question and needs to be adapted for every hypothesis test. Therefore, we did so to answer new questions during the last half year of the project (Y2.5). Nonetheless, the spirit behind it is clear, and we expect it to become a usual approach that speeds up the development of the field of RS of plant biodiversity.

The development of these frameworks was thorough. We assessed the impact of different modeling choices during Y1. For example, we evaluated how plant functional traits' covariance was accounted for or ignored in the simulations. We compared the results of three different ways of generating random distributions of plant traits: 1) Latin Hyper Sampling, which includes no covariance, 2) Gaussian

Mixture Models (GMM) trained with plant trait databases and 3) direct sampling from databases. We concluded that covariance was essential in the simulations and that GMMs fitted with the LOPEX (Hosgood et al. 1994) and ANGERS (Feret et al. 2008) databases could offer the best compromise. We included additional constraints for variables missing in these databases to avoid unrealistic simulations that spuriously inflated functional diversity and metrics correlations. Specifically, we constrained anthocyanin and senescent pigment contents as a function of chlorophyll content.

Another critical consideration in the simulation framework was ensuring the generation of different levels of plant functional diversity. Truncated sampling allowed us to limit the variability ranges of plant functional traits to various degrees. However, this was not enough to provide realistic simulations. Using ecological theory, we split simulations into "similar" and "dissimilar" species mixed into the same community, representing subcommunities competing for the same or exclusive resources, respectively. We first defined species pools that included different fractions of similar and dissimilar species. From each pool, we generated several communities by varying the dominant species, the dominance level, and the fraction of "similar" and "dissimilar" species (Figure 2). The coherence of the simulations was later confirmed using remote sensing imagery (Sentinel-2 and DESIS, RD1.1.c) over the biodiversity monitoring network FunDivEUROPE (Baeten et al. 2013).

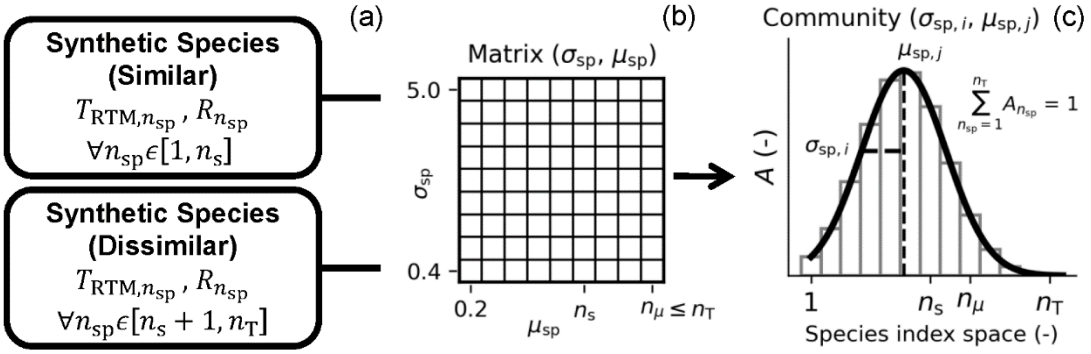

Figure 2. Generation of several (81) synthetic communities from the same species pool. (a) Pool of n_s similar and n_{ds} dissimilar species adding up to n_T; each species is labeled with an integer n_{sp} and characterized by a specific set of field plant traits (T_{RTM}) and the corresponding reflectance factor (R). (b) Communities matrix presenting the 81 combinations of the median (μ_{sp}) and the standard deviation (σ_{sp}) of the Gaussian distribution used to define the relative species abundance (A) of each community. i and j are row and column indices of the matrix; only a fraction of the dissimilar species is allowed to dominate communities so that μsp ranges up to $n_\mu \leq n_T$. (c) Relative species abundance distribution of one of the communities (Pacheco-Labrador et al. 2022b).

While this approach was suitable for assessing the relationships between functional diversity metrics (FDMs) estimated from remote information or plant functional traits, it was suboptimal for evaluating methods for functional diversity partition at different spatial scales. These are intra-community (α-diversity), inter-community (β-diversity), and total diversity (γ-diversity). Diversity partitioning methods required larger species richness and turnover between communities (β-diversity) in the simulations to be thoroughly tested. This was achieved by modifying

how communities were generated and the maximum species richness, as shown in Figure 3.

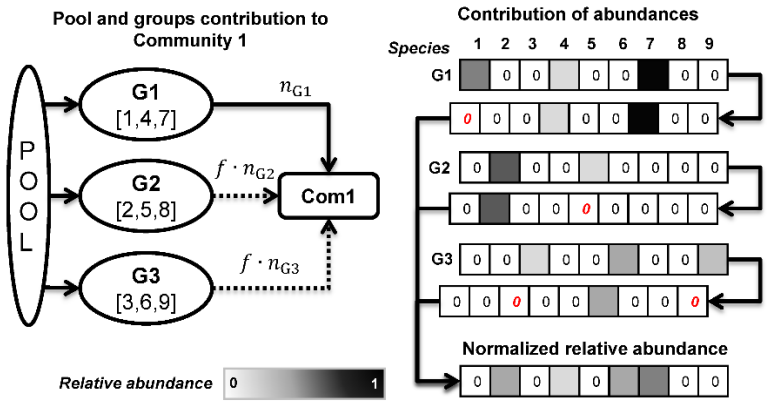

Figure 3. Schematic representation of the simulation of one of the communities of an image or region. Nine species are simulated and labeled from 1 to 9. The species pool is split into three groups, not necessarily evenly (*G*). Only G_1 contributes with all the species to the community, whereas the others provide only a fraction (*f*) of their species (left). Detail on the relative contribution of the species provided by each group, some species' abundance is set to 0 (red fonts) to increase β-diversity. Finally, the relative abundances are normalized (right).

Once plant functional traits and species communities were defined, their spectral properties had to be simulated. The frameworks started working with the radiative transfer model PROSAIL (Jacquemoud et al. 2009), which was able to represent hyperspectral reflectance factors (*R*). However, during Y1, we changed to the integrated model of soil-canopy spectral radiances, photosynthesis, fluorescence, temperature, and energy balance: SCOPE (van der Tol et al. 2009) to explore the use of more signals beyond reflectance factors. SCOPE allowed us to assess the capability of sun-induced chlorophyll fluorescence (SIF) at O_2-A and O_2-B atmospheric absorption features (760 and 687 nm, respectively) to infer plant functional diversity. The advantage of this signal over reflectance factors is that it could provide additional information about physiological diversity.

In addition, to speed up the simulations, we trained emulators or statistical surrogates of the physical models (Gómez-Dans et al. 2016). We tested different machine learning algorithms and eventually selected shallow Neural Networks due to their balance between accuracy, lightweight, and fast prediction capabilities. We also developed emulators for other models, such as senSCOPE (Pacheco-Labrador et al. 2021), a SCOPE version adapted to Mediterranean and semi-arid ecosystems, or the 3D radiative transfer model FLIGHT (North 1996). Figure 4 summarizes the validation statistics for the reflectance factors Neural Network emulators of senSCOPE and FLIGHT, which proved more challenging. Eventually, we mostly used the SCOPE emulator to represent unspecific natural ecosystems because its accuracy and precision were higher than for FLIGHT.

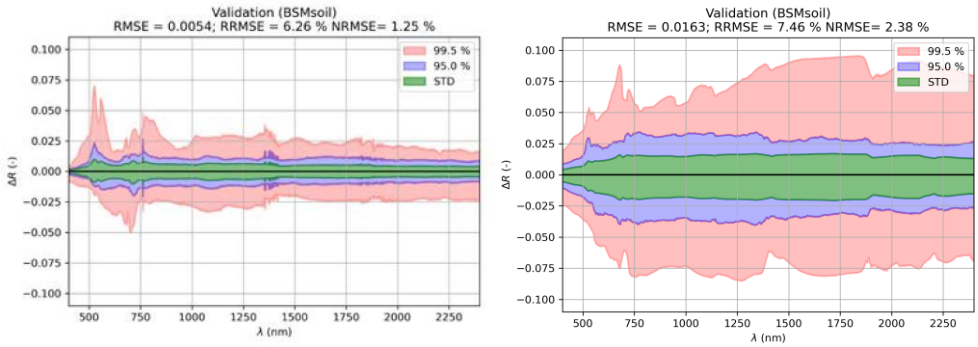

Figure 4. Validation of senSCOPE (left) and FLIGHT 3D (right) radiative transfer emulators, predicting surface reflectance factors (*R*). The spectral distributions of the difference (*Δ*) between predicted and simulated reflectance are shown together with summarizing statistics (*RMSE*: Root Mean Squared Error, *RRMSE*: Relative Root Mean Squared Error, *NRMSE*: Normalized Root Mean Squared Error).

Moreover, to assess the impact of sensor characteristics on the estimation of plant functional diversity, we implemented the representation of three remote sensing features affecting the relationships between field and remote sensing FDMs:

1) Spectral configuration: We simulated full-hyperspectral (as provided by the RTM), DESIS (German Aerospace Center (DLR) / Teledyne Brown Engineering Company (Huntsville, Alabama, USA)), and Sentinel-2 MSI (ESA, Copernicus Programme) spectral bands. In a second work, we also included QuickBird-2 (DigitalGlobe Inc.) to limit the spectral information even more.
2) Spatial resolution: Spatial resolution was abstracted to simplify the already complex simulations. It was defined as *the sensor's capability to discriminate individual species*, enabling the mixture of different species for suboptimal spatial resolutions where not all species could be individually distinguished. To do so, we mixed the community species' traits and spectral variables so that the signal perceived by the sensor resulted from a combination of different species.
3) Sensor noise: We added different levels of relative random noise to spectral signals and field plant traits.

Figure 5 shows an example. Figure 5a-c presents the relative abundance of the species of a regional pool in a given community, their spectral properties, and their plant functional traits (T_{RTM}), respectively. Species 1-6 are similar and feature alike plant functional traits and spectral reflectance; in the community simulated, species 3 is the most abundant. Species 7-9 are dissimilar and feature more distinct functional and spectral properties. These are initially not present in the "field plot" where the community shown is characterized in the field. However, as remote sensing resolution decreases, pixels can sample outside the given field plot or community and capture new species (Figure 5d,g). At suboptimal spatial resolution, the sensor perception of abundances and spectral properties changes from "pure" species to mixtures of several species (Figure 5d,e,g,h). Figure 5f,I show how hyperspectral reflectance is convolved to the spectral bands of Sentinel-2 and DESIS sensors, and relative noise of different levels is added.

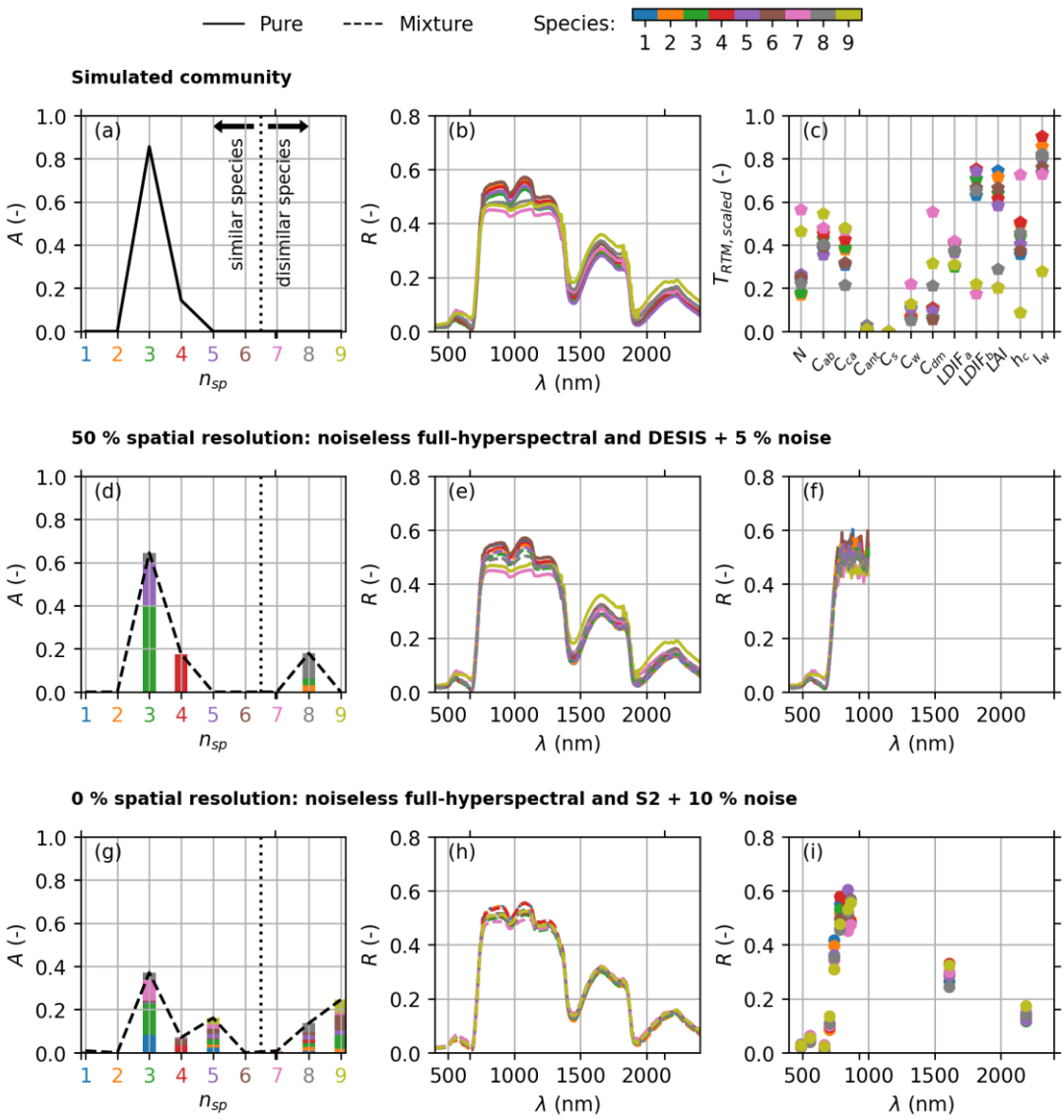

Figure 5. Example of the simulation and effect of different remote sensing features on one of the synthetic communities simulated. The first row presents the original abundances (*A*) (a), species reflectance factors (*R*) (b), and field plant traits (T_{RTM}) scaled within the bounds set for the simulation (c). In the abundance subplots (first column), the black-pointed line separates similar (on the left) from dissimilar species (on the right). The color assigned to each species' number (n_{sp}) identifies the corresponding reflectance factors and traits in the remaining subplots. Solid lines represent pure species, whereas dashed lines represent spectral mixtures due to spatial resolution degradation. The second row degrades spatial resolution so that only 50 % of the species in the pool can be discriminated, leading to new estimates of species abundances (d); the color bars represent the contribution of each species to the new species abundance, observed by the remote sensor. Sensed reflectance factors, full-hyperspectral and noiseless (e), or convolved to DESIS spectral bands with a 5% random noise (f). The third row degrades spatial resolution so that none of the species can be identified, leading to new estimates of species abundances (g); the color bars represent the contribution of each species to the new species abundance observed by the remote sensor. Sensed reflectance factors, full-hyperspectral and noiseless (e), or convolved to Sentinel-2 MSI spectral bands with a 10% random noise (i) (Pacheco-Labrador et al. 2022b).

We used this simulation framework to analyze plant functional and spectral diversity relationships. To do so, we synthesized these multidimensional datasets into single scalars that summarize different aspects of their variability, the functional diversity metrics (FDMs). Over time, we have integrated different FDMs into the framework. First, we used metrics characterizing diversity at the community scale (α-diversity), such as functional richness, evenness, and divergence (Mason et al. 2005) and Rao's quadratic entropy *Q* (Botta-Dukát 2005) implemented the metrics provided by the R language package "FD" from Laliberté and Legendre (2010) (Functional richness, dispersion, divergence, evenness, and Rao's *Q*). Moreover, in Y2, we included the computation of the parametric version of Rao's *Q* proposed by Rocchini et al. (Rocchini et al. 2021). At the end of Y2, we also included methods and metrics suitable for partitioning diversity at various scales (α, β, and γ-diversity). Specifically, the analysis of variance (Laliberté et al. 2020) and diversity partitioning based on the Rao *Q* index (de Bello et al. 2010). However, diversity partitioning suffers from biases in the estimation of β-diversity when diversity indices (such as the metrics abovementioned), and not their equivalent numbers, are used. The equivalent numbers are formulation-independent diversity metrics with mathematical properties enabling unbiased diversity partitioning (Jost 2006, 2007). In the case of Rao *Q*, the computation of its equivalent number (Q_{eq}) requires normalizing the dissimilarity metric exploited by the Rao *Q* index (the Euclidean distance) to prevent α-diversity larger than γ-diversity. This normalization is often carried out in ecological studies by using the maximum dissimilarity found in the plant trait datasets analyzed. However, this approach is not feasible in the context of global remote sensing analysis since finding the maximum dissimilarity requires processing (huge and ever-growing) global datasets every time a map is produced or new information arrives. We solved this problem by developing a new global normalization approach that can be applied to several FDMs leading to comparable values (RD1.1.e). This way and beyond the project expectations, oBEF-Accross2 has achieved a new relevant contribution to the remote sensing of plant biodiversity. The method is also valuable in other context, such as ecology analysis.

RD1.1.b. Challenging the links between spectral and functional diversity

With the consolidation of the first simulation framework, we aimed to answer four relevant questions in the field of remote sensing of plant functional diversity:

1) Which FDMs can link plant functional and spectral diversity?
2) Should we use reflectance factors or optical traits?
3) Are FDMs comparable at local (e.g., one image) and global (e.g., multiple images separately analyzed) scales?
4) What is the effect of remote sensing features (spectral configuration, spatial resolution, uncertainties)?

To answer these questions, we compared different FDMs computed from spectral traits (reflectance factors *R* or, in early analyses, SIF) or optical traits ($T_{optical}$, plant traits estimated from spectral information) against FDMs calculated from plant traits (inputs of the radiative transfer model, T_{RTM}) as if sampled in the field. Notice that optical traits are strongly linked with the Essential Biodiversity Variables

(Skidmore et al. 2021). This way, we covered the two main approaches used in remote sensing to infer plant functional diversity (Wang and Gamon 2019). Moreover, we imposed three levels of three different factors (remote sensing features): spectral configuration (full-hyperspectral, DESIS, and Sentinel-2), spectral resolution (100, 50, or 0 % of the species discriminated by the remote sensor), and uncertainty (relative noise levels of 0, 5, and 10 %). Figure 6a summarizes in part the workflow of these analyses. The simulation framework produced artificial communities of plant species from where we computed the abovementioned FDMs using 1) the vegetation traits (T_{RTM}), 2) spectral traits, and 3) optical traits estimated via radiative transfer model inversion ($T_{optical}$). Figure 6b presents the validation of the modeling framework and the conclusions obtained using Sentinel-2 and DESIS imagery over the biodiversity plots of the biodiversity monitoring network FunDivEUROPE (Baeten et al. 2013).

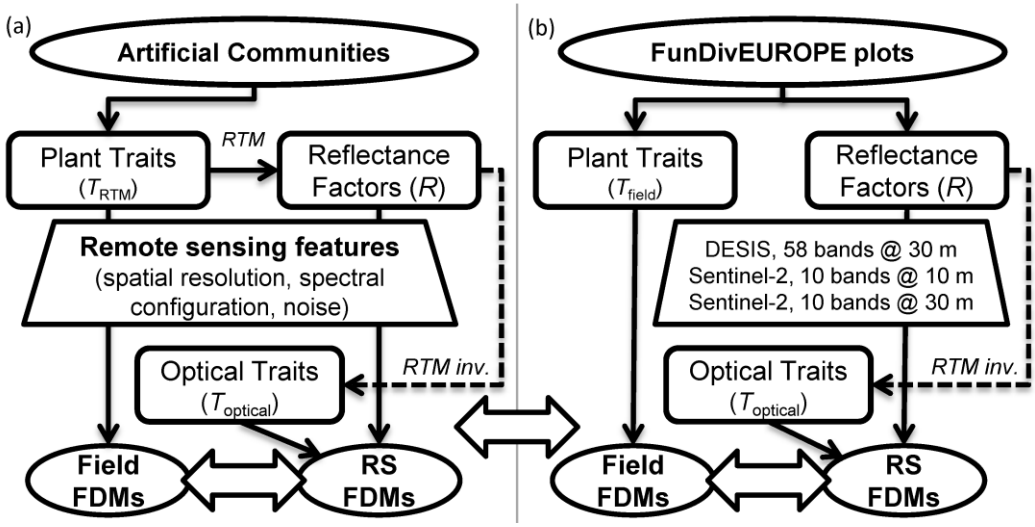

Figure 6. Workflow representing the analyses performed using the simulation framework and the observational datasets of the FunDivEUROPE network (Pacheco-Labrador et al. 2022b).

The first analyses showed that FDMs computed with *R* or *F* separately or together behaved similarly, whereas the spatial resolution seemed to play a more important role. Since optical sensors' spatial resolution is less limited than fluorescence imagers, we decided to simplify our analyses and focus on the reflectance factors. Still, fluorescence analyses were useful and guided the dedicated study case using airborne SIF imagery (RD1.1.f). Radiative transfer model inversion used numerical optimization to estimate plant functional traits from the spectral reflectance factors as observed by the sensor at each resolution. Inversion was accelerated using an emulator. We used a second emulator trained with an independent dataset to ensure a certain "model error" in the estimation (the discrepancy between the radiative transfer model representation and reality). Still, the same emulator used in the simulations was also inverted to quantify this effect.

Simulations comprehended 1000 regions, each made of 81 communities (Figure 7a-d). First, we defined the species of a regional pool by sets of plant traits and the corresponding reflectance factors (Figure 7a,b) and sampled them into the

communities of that region (Figure 7c). Then, we imposed various remote sensing features (3 factors x 3 levels), producing 27 simulations. The individual analysis of each region would be equivalent to ecological biodiversity studies or single-image analysis. This configuration allowed us to assess the FDMs relationships were analyzed in two different ways:

1) At the local scale (region by region or image per image, Figure 7e), by generating distributions of different statistics (e.g., R^2) summarized by their median and confidence interval.
2) At the global scale (all the regions together, Figure 7f), by getting a single statistic for all the regions.

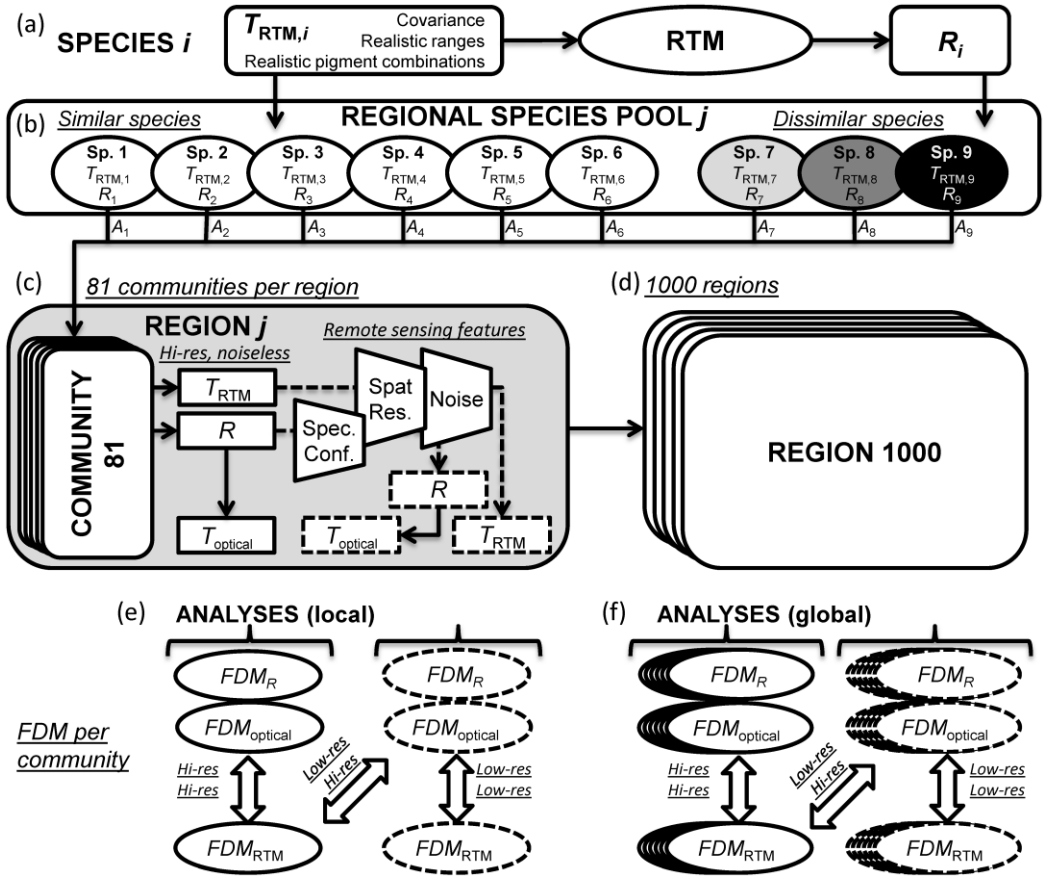

Figure 7. Detailed simulation and analysis workflow. Each species (*i*) is defined by a plausible set of field plant traits (T_{RTM}), the input of a radiative transfer model (RTM) that predicts the associated reflectance factor (*R*) (a). Several species (9 in this example) are gathered within a regional species pool (b). Some species feature traits with close or similar values (similar species), whereas others feature dissimilar trait values (dissimilar species). Then, the species from the pool are sampled with different abundances (*A*) to produce 81 communities per region (c); the original traits and reflectance factors (solid lines) are transformed by different remote sensing features (dashed lines). In both cases, the plant traits are also estimated from the optical signals via radiative transfer model inversion (optical traits, $T_{optical}$). In total, 1000 regions are produced from a corresponding number of species pools (d). Functional diversity metrics (FDM) are computed from the abundances and either the field vegetation traits (FDM_{RTM}), the optical traits ($FDM_{optical}$), or the spectral reflectance factors (FDM_R) of each community. The relationships between the FDMs at different spatial resolutions are compared for each region (e) and all the regions at the same time (f) (Pacheco-Labrador et al. 2022b).

The underlying reason is not trivial. FDMs require removing traits' magnitude and autocorrelation via standardization and dimensionality reduction of the *n*-dimensional trait space. The literature recommends applying these transformations to the entire database, which is usual in ecological studies handling limited datasets. However, this approach is not reasonable for ever-growing global remote sensing datasets, and single-image analysis remains a more operational alternative. Therefore, an unsolved critical question was whether FDMs computed from individual images are comparable and can be used to build global products of plant functional diversity. In addition, we took advantage of the different spatial resolutions simulated to assess the effect of the scale when comparing remote sensing and field estimates of plant functional diversity Figure 7e,f. First, we compared high spatial resolution field FDMs with the different spatial resolutions simulated for the remote sensing FDMs. The former is the classical scheme used to calibrate and validate remote sensing products. Field studies characterize the plot's contents that are later compared with a pixel or region of interest of a satellite image. However, in biodiversity studies, the variability of several pixels is compared with field data, which requires unusual sampling schemes where field data capture the variability of several nearby plots separately, mimicking the window of pixels used to compute the FDM (Hauser et al. 2021). For this reason, we simulated such field datasets by mimicking the remote sensing resolution with field datasets.

The simulation framework provided complete control over the main factors affecting the relationships between remote sensing and field functional diversity estimates (i.e., FDMs, spectral and optical traits, comparison scales, sensor features, etc.). This control and the factorial simulations approach allowed us to understand their effect on the FDM relationships and, therefore, the strengths and weaknesses of remote sensing to infer plant functional diversity from space. Furthermore, this approach overcame the lack of overlap of these factors found in the (young) literature on this topic.

Our analyses departed from comparing field and remote sensing FDMs under ideal conditions (hyperspectral, high spatial resolution, and noiseless datasets). They showed the capability of the different FDM formulations to link the diversity estimated from plant functional traits and spectral (Figure 8) or optical (Figure 9). We always performed the comparisons at the local and global scales (regression lines). This first analysis already identified the FDMs that are not suitable for remote sensing studies (functional evenness (*FEve*), divergence (*FDiv*), and Rao's *Q* with α=0). Moreover, they indicated that the optical traits performed slightly better than spectral traits, despite the high retrieval uncertainties for some parameters. These results suggest that equifinality might not be a critical issue for functional diversity analysis since exchanges of parameter values might still retain their variability. Finally, the comparison of scales showed a large variability of the correlations at the local scale, which was, on average, slightly larger than at the global scale. This last result is capital since it suggests that individually processed images (maps of FDMs) could be coherently used to generate global remote sensing products of plant functional diversity. It also could explain why former studies found mild correlations for FDMs that were here discarded for remote sensing use in our analyses (e.g., Schneider et al. (2017)).

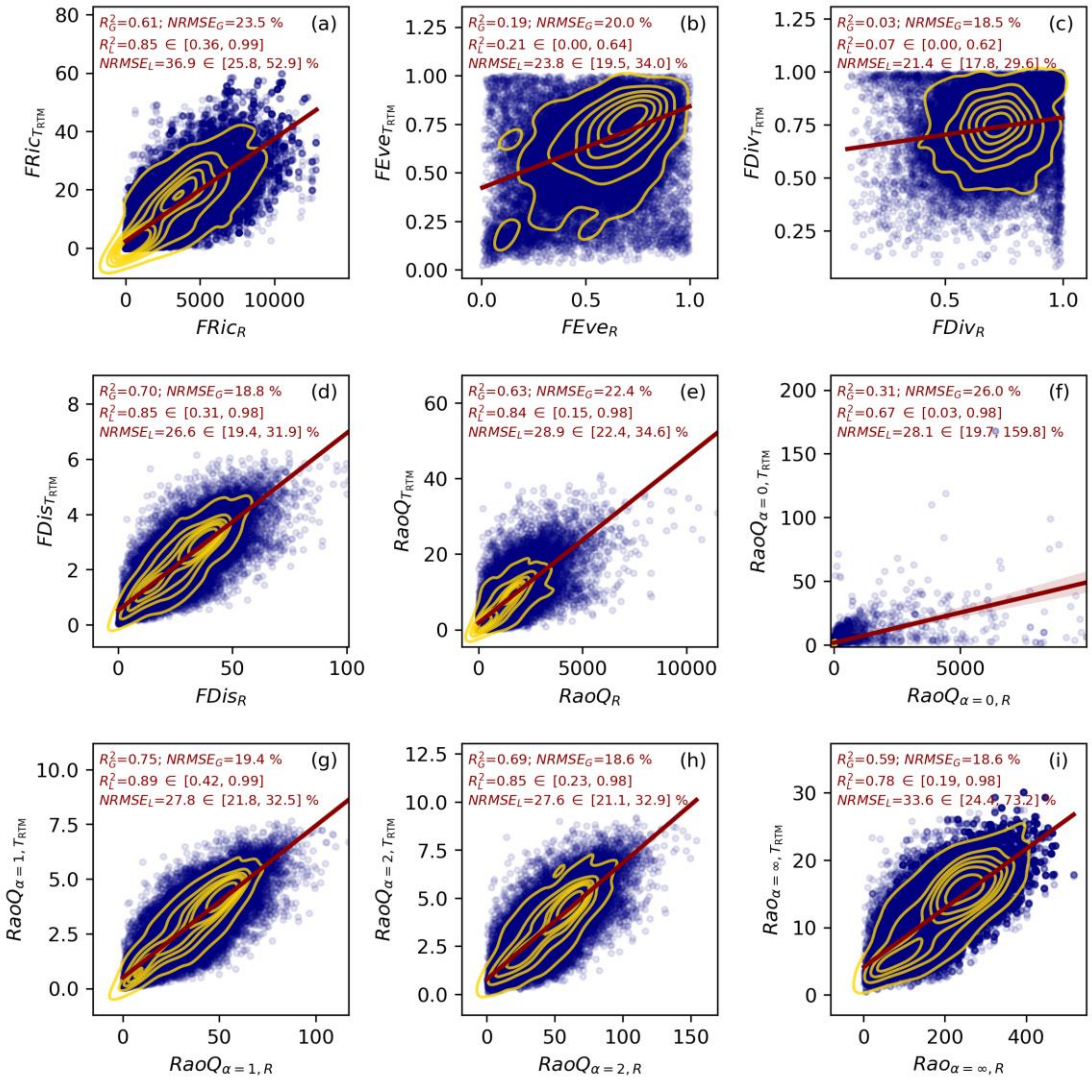

Figure 8. Relationship between the functional diversity metrics computed from the reflectance (subscript "*R*") factors and field plant traits (subscript "T_{RTM}") using the *dbFD* package (a-e) or the parametric Rao's *Q* formulation with different values of the parameter α (f-i). Regression lines summarize the comparison at the global scale; the shaded areas around the regression lines represent the 95 % confidence interval of the line. Each subplot includes the statistics of the relationship at the global scale (on top, subscript "G") and the median and 95 % confidence interval of the statistics at the local scale (below, subscript "L") (Pacheco-Labrador et al. 2022b).

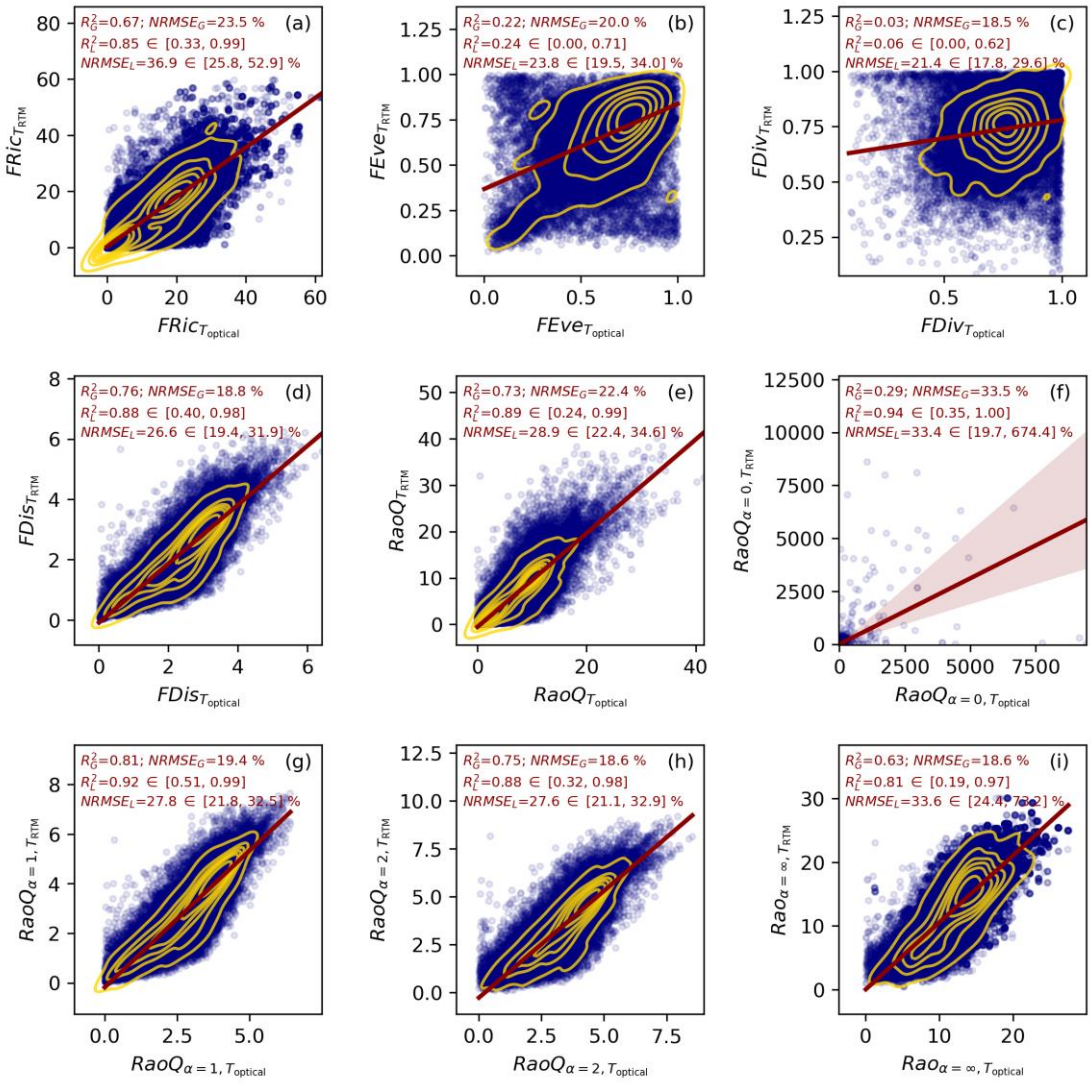

Figure 9. Relationship between the functional diversity metrics computed from optical traits estimated via radiative transfer model inversion (subscript "$T_{optical}$") and field plant traits (subscript "T_{RTM}") using the *dbFD* package (a-e), or the parametric Rao's *Q* formulation with different values of the parameter α (f-i). Two different emulators simulated the reflectance factors and estimated the optical traits to induce model error. Regression lines summarize the comparison at the global scale; the shaded areas around the regression lines represent the 95 % confidence interval of the line. Each subplot includes the statistics of the relationship at the global scale (on top, subscript "G") and the median and 95 % confidence interval of the statistics at the local scale (below, subscript "L") (Pacheco-Labrador et al. 2022b).

The findings of this first study are genuine and very relevant. However, they had to be matured and tested under suboptimal conditions where part of the information is altered or lost due to inherent features of the remote sensing technique. Figure 10 shows the results of this robustness test, where the different metrics and methods (spectral or optical traits) are assessed at the local and global scales. The first two rows compare field and reflectance-based FDMs, whereas the last two rows compare field and optical trait-based FDMs. Here, we also test the effect of the field sampling scheme used to validate the remote sensing estimates. We compared field data at high spatial resolution (hi-res) with different remote sensing

resolutions in rows one and three. In contrast, we adapted field resolution to the remote sensor (RS-res) resolution in rows two and four.

From these analyses, we were able to extract the following conclusions:

1) The spatial resolution is the most limiting factor in the remote estimation of plant functional diversity. Matching field and remote sensing resolutions can alleviate the loss of correlation between FDMs. This result implies that validating remote sensing estimates of plant functional diversity demands specific field sampling designs.
2) The spectral trait approach (i.e., using reflectance factors) is only slightly affected by the spectral configuration of the sensor. On the contrary, despite the larger potential shown under ideal conditions, the optical trait approach is more sensitive to noise and reduced spectral information (multi-spectral sampling and lack of SWIR bands). These results make it recommendable using the spectral trait approach only with VSWIR hyperspectral missions such as EnMAP, PRISMA, SBG, CHIME, *etc*, and the spectral trait approach for any other mission.
3) In most cases, local-scale comparisons show, on average, higher correlations than global-scale comparisons; still, the large variability of correlations must be considered when analyzing local datasets.
4) Noise and spatial resolution degradation can spuriously inflate the correlations of the FDMS: *FEve*, *FDiv*, and *FRic*, especially when field and remote sensing resolutions are matched.

Evaluating the FDM relationships under suboptimal conditions in a modeling framework has allowed answering questions out of the reach of local and empirical studies initially foreseen. These analyses have 1) revealed the role of the spatial and the spectral resolution of the different sensors, 2) clarified the most suitable approaches for the different mission types, 3) proven that individual image-based analysis enables the generation of global plant functional trait products, and 4) identified the most suitable metrics for remote sensing analysis (Rao *Q* and functional dispersion (*FDis*), followed by *FRic* with some cautions).

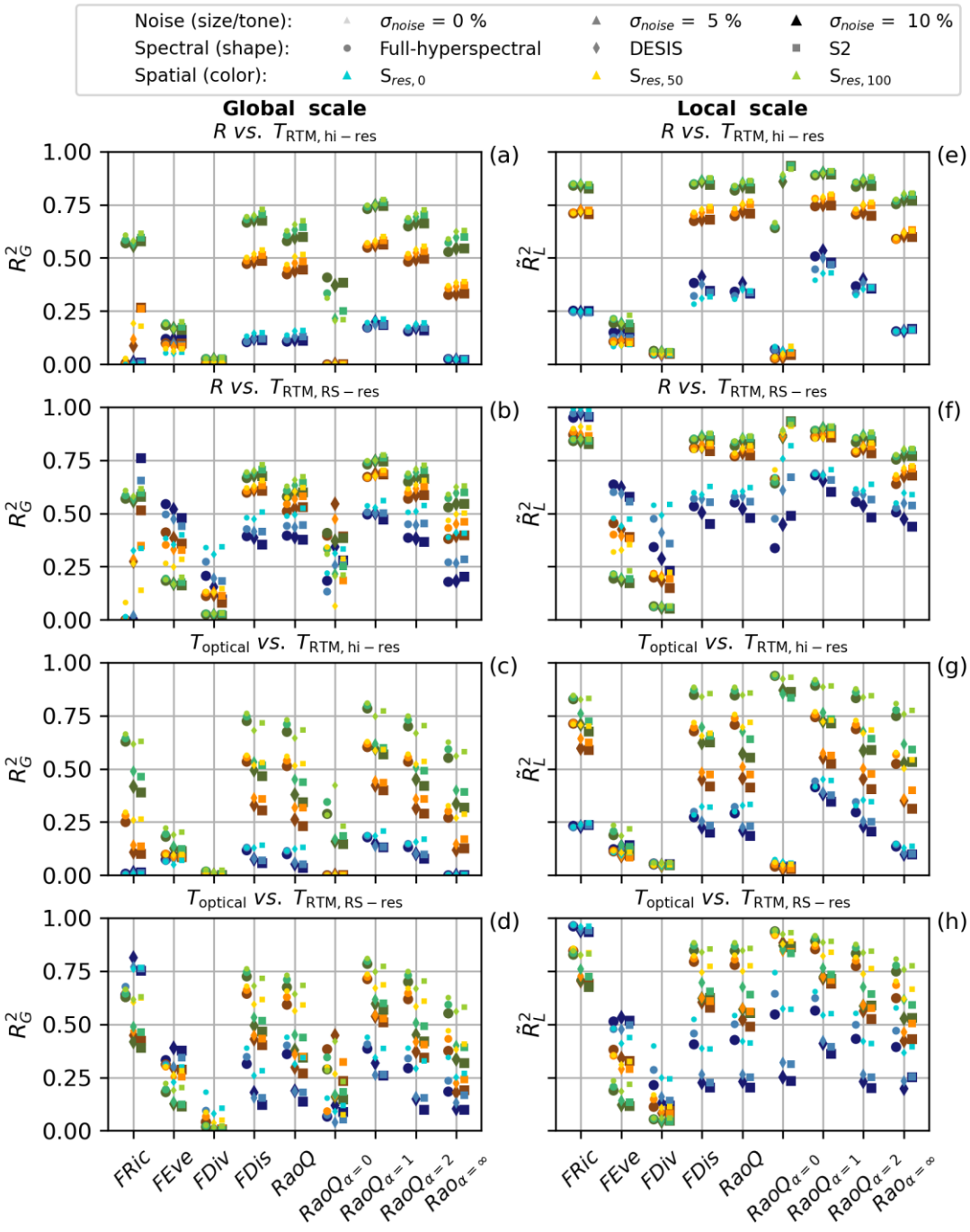

Figure 10. Evaluation of remote sensing features on the relationships between functional diversity metrics. Metrics computed from field plant traits (T_{RTM}) are compared with remote sensing metrics computed either from reflectance factors (R) or estimated optical traits ($T_{optical}$). The left column presents R^2 of the relationships between metrics compared at the global scale (R_G^2), the right column shows the median R^2 of the evaluation at the local scale ($\tilde{R}_L^2$). Functional diversity metrics computed from reflectance factors at sensor resolution are compared with field metrics at maximum spatial resolution (hi-res), representing the mismatch between remote sensors and field surveys (a, e) and remote sensing resolution (RS-res) mimicking remote sensing-oriented field surveys (b, f). Functional diversity metrics computed from estimated optical traits at senor resolution are compared with field metrics at maximum spatial resolution (hi-res) (c, g) and remote sensing resolution (RS-res) (d, h). Markers show different spectral configurations; color ranges indicate spatial resolution, whereas marker size and tone represent noise level (Pacheco-Labrador et al. 2022b).

RD1.1.c. Quantifiying functional diversity with space-borne remote sensing imagery

In Y1, we generated observational remote sensing and field datasets initially intended to develop new methods for estimating plant functional diversity from space. Preliminary empirical analyses compared the potential of hyperspectral and multi-spectral information (Figure 1). We tested different approaches with simulated and observational datasets to determine the best options to estimate plant functional diversity from spectral information. In Y2, we demonstrated that directly comparing some FDMs computed from spectral and plant functional traits could provide the most reliable estimates. We re-directed the development work towards modeling due to its greater potential to answer fundamental questions. Thus we converted these datasets into a validation tool for the simulations' plausibility and the correctness of the conclusions obtained.

Observational data focused on the network FunDivEUROPE. FunDivEUROPE is a biodiversity monitoring experiment consisting of 30 x 30 m monitoring plots deployed in forests of six European countries (Baeten et al. 2013). We focused on the three countries where in addition to taxonomical and structural traits, foliar traits had also been sampled (Benavides et al. 2019a; Benavides et al. 2019b): Spain (SPA), Romania (ROM), and Finland (FIN). oBEF-Accross2 built on the results of oBEF-Accross, the precursor project that demonstrated Sentinel-2 able to infer plant functional diversity in these plots using non-parametric regression approaches (Ma et al. 2019).

FunDivEUROPE database was enriched with DESIS imagery (German Aerospace Center (DLR) / Teledyne Brown Engineering Company (Huntsville, Alabama, USA)) was tasked and cured through the "DESIS Data Announcement of Opportunity" *EBioIDEA: Enhancing Biodiversity Inventories with DESIS Imagery Analysis* proposed by oBEF-Accross2 MPI members and other collaborators. This proposal was written and submitted during Y1. DESIS is a 30 m spatial resolution hyperspectral visible-to-near infrared (VNIR) imager onboard the International Space Station. These datasets were used for preliminary analyses. In Y2, we also exploited Sentinel-2, a multi-spectral visible-to-short wave infrared (VSWIR) imager, whose data were pan-sharpened at 10 m (Ma et al. 2019)) and compared the capabilities of both sensors. However, field and remote sensing had been acquired in different years, and there was a particularly large gap between Sentinel (2015) and DESIS (2020) acquisitions. For this reason, in Y2.5, additional Sentinel-2 imagery was downloaded and processed to enable a comparison using coetaneous imagery from both sensors.

In Y2, we assessed the capability of FDMs computed from DESIS and Sentinel-2 (subsection RD1.1.a) to directly correlate with functional FDMs and taxonomical diversity metrics (i.e., species richness (*S*) and Shannon index (*H*)) computed from FunDivEUROPE field data. Since the DESIS footprint is limited in latitude, we could only use the sites of Spain and Romania (Finland, where foliar traits had also been sampled, could not be imaged by this sensor). In Y2.5, we also compared Sentinel-2 imagery from 2020, coetaneous to DESIS imagery, confirming the validity of previous findings. In addition, we reduced the differences in spatial resolution existing between Sentinel-2 (10 m, $S2_{10}$) and DESIS by resampling the multispectral imager to 30 m ($S2_{30}$). This analysis contributed to validating simulation results where spatial resolution appeared as the sensor feature controlling FDMs relationships the most. Figure 11 presents the

different imagery used in FunDivEUROPE over a plot in Spain. As the 30 m resolution equals plot size, an spatial mismatch forcibly exists between DESIS and $S2_{30}$ with field data, a usual situation since biodiversity plots have not been designed for the validation of remote sensing estimates.

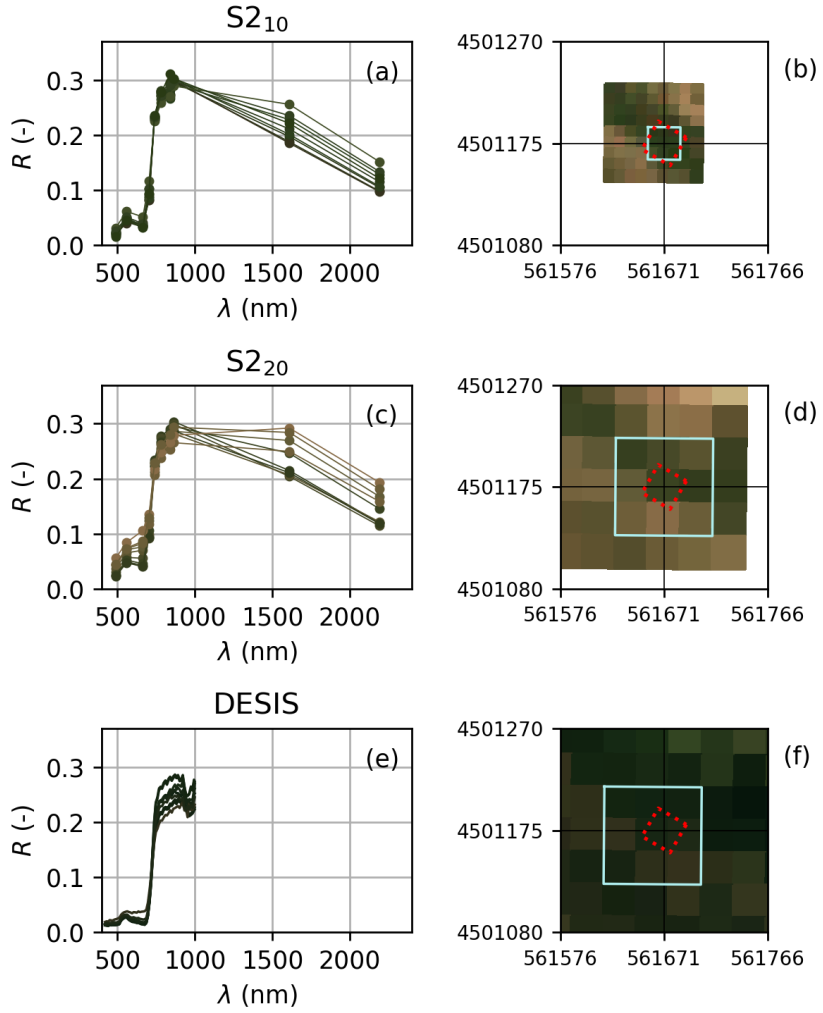

Figure 11. Example of the remote sensing data used in one of the FunDivEUROPE sites in Spain (SPA01). Spectra of the 3 x 3 pixels window used to compute the functional diversity metrics (first column) and red-green-blue composition of the clips around the site (second column) together with the plot (red dashed line) and the 3 x 3 pixels window (pale blue) used to compute functional diversity metrics. Sentinel-2 MSI @ 10 m pixel in 2015 ($S2_{10}$, first row), Sentinel-2 MSI @ 30 m pixel in 2015 ($S2_{30}$, second row) and DESIS @ 30 m pixel in 2020 (third row). Spectra and imagery pixel colors are matched (Pacheco-Labrador et al. 2022b).

We used a radiative transfer model inversion scheme similar to the one implemented for the simulations (RD1.1.b) to validate the results using the optical trait approach with RS imagery. Trait estimation required the additional calculation of the observation and illumination angles and aerosol optical thickness from imagery. Field data showed that, as in the simulations, uncertainties and equifinality were large in some of the trait estimates. However, the relationships between observed and predicted parameters were significant. The analysis of observational data (Figure 12) was coherent with the simulations (Figure 10), thus proving their validity. *RaoQ* and

FDis metrics significantly correlated with field metrics when the spatial resolution was enough to sample within the reference plots ($S2_{10}$). Therefore, $S2_{30}$ nor DESIS could not offer significant correlations, or these were found (for $S2_{30}$) in FDMs prone to spuriousness, as shown by the simulations.

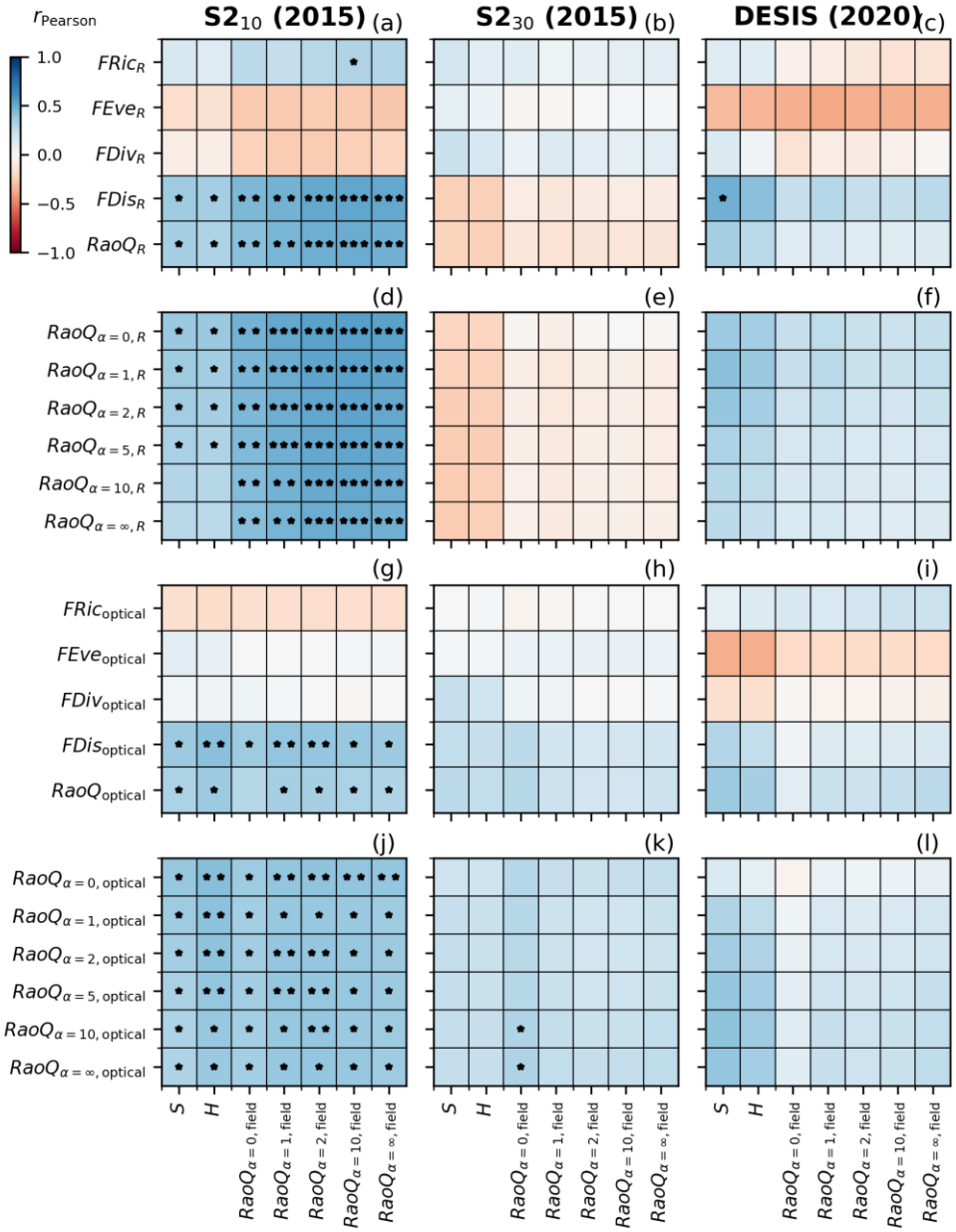

Figure 12. Pearson correlation coefficient between taxonomical and functional diversity metrics computed from field plant traits (subscript "field", *x*-axis) and functional diversity metrics computed from remote sensing information (*y*-axis): the reflectance factors (subscript "*R*", first two rows) or the optical traits (subscript "optical", last two rows). In each case, the *dbFD* package metrics are presented first, and the parametric Rao's *Q* afterward. The statistics correspond to Sentinel-2 MSI @ 10 m spatial resolution ($S2_{10}$, first column), Sentinel-2 MSI @ 30 m spatial resolution ($S2_{30}$, second column), and DESIS at 30 m spatial resolution (DESIS, third column). Sentinel-2 imagery was acquired in 2015. Asterisks indicate the significance of the correlation (two-tailed) according to its p-value (*p*): * → $p < 0.001$, ** → $0.001 \leq p < 0.01$, and ** → $0.01 \leq p < 0.05$ (Pacheco-Labrador et al. 2022b).**

Intermediate results of the DESIS analyses were presented via oral communication in the "1st DESIS User Workshop" in September 2021, submitted for publication in the conference proceedings in November 2021, and published after review in 2022 (Pacheco-Labrador et al. 2022c). The complete analysis of the observational datasets and the simulation framework was presented in the A2.01.1 Biodiversity session of the ESA Living Planet Symposium in Bonn in May 2022 (Pacheco-Labrador et al. 2022a). This presentation got remarks and an expression of interest from the Scientific PI of the future hyperspectral ESA mission CHIME, Dr. Marco Celesti. This joint work, summarized in sections RD1.1.a-c, was submitted to *Remote Sensing of Environment* in October 2021, reviewed twice, and eventually published in July 2022 (Pacheco-Labrador et al. 2022b).

RD1.1.d. Importance analysis of plant functional traits' diversity role in spectral diversity

oBEF-Accross2 exploited the mechanistic base of the simulation framework developed to improve our understanding of the relationships between plant traits and spectral diversity. Already in Y1, we carried out different exploratory analyses to understand 1) the role of the plant functional traits on spectral diversity and thus the relationships between spectral and plant functional diversity; and 2) the capability of spectral identity (the community-weighted average) and diversity (community-weighted standard deviation or FDMs) to predict plant functional diversity. We evaluated different statistical approaches, such as Global Sensitivity Analysis (GSA) or SHAP (SHapley Additive exPlanations), performed over machine learning models trained with the simulated data (Neural Networks, Gaussian Process Regression, Random Forest and Kernel Ridge Regression). Results were not strongly conclusive at the time but highlighted the role of leaf area index in the relationships analyzed.

In addition, we fit different predictive models to estimate plant functional diversity (represented by different FDMs) from spectral identity and diversity data. First, we performed simple exploratory analyses to assess the correlation between each spectral band's identity and diversity with plant FDMs. Then we used more sophisticated approaches, such as LASSO, and performed feature selection using Least Angle Regression ("LARS") based on the Akaike information criterion (AIC). Unfortunately, these early results did not offer robust correlations, meaning that, at least at the global scale, these approaches might not be suitable to produce generalizable estimates of plant functional diversity (Figure 13). Nevertheless, this was one of the first indications that investing in simulations rather than data-driven approaches could provide a better insight into remote sensing techniques' potential and limitations to monitoring plant biodiversity.

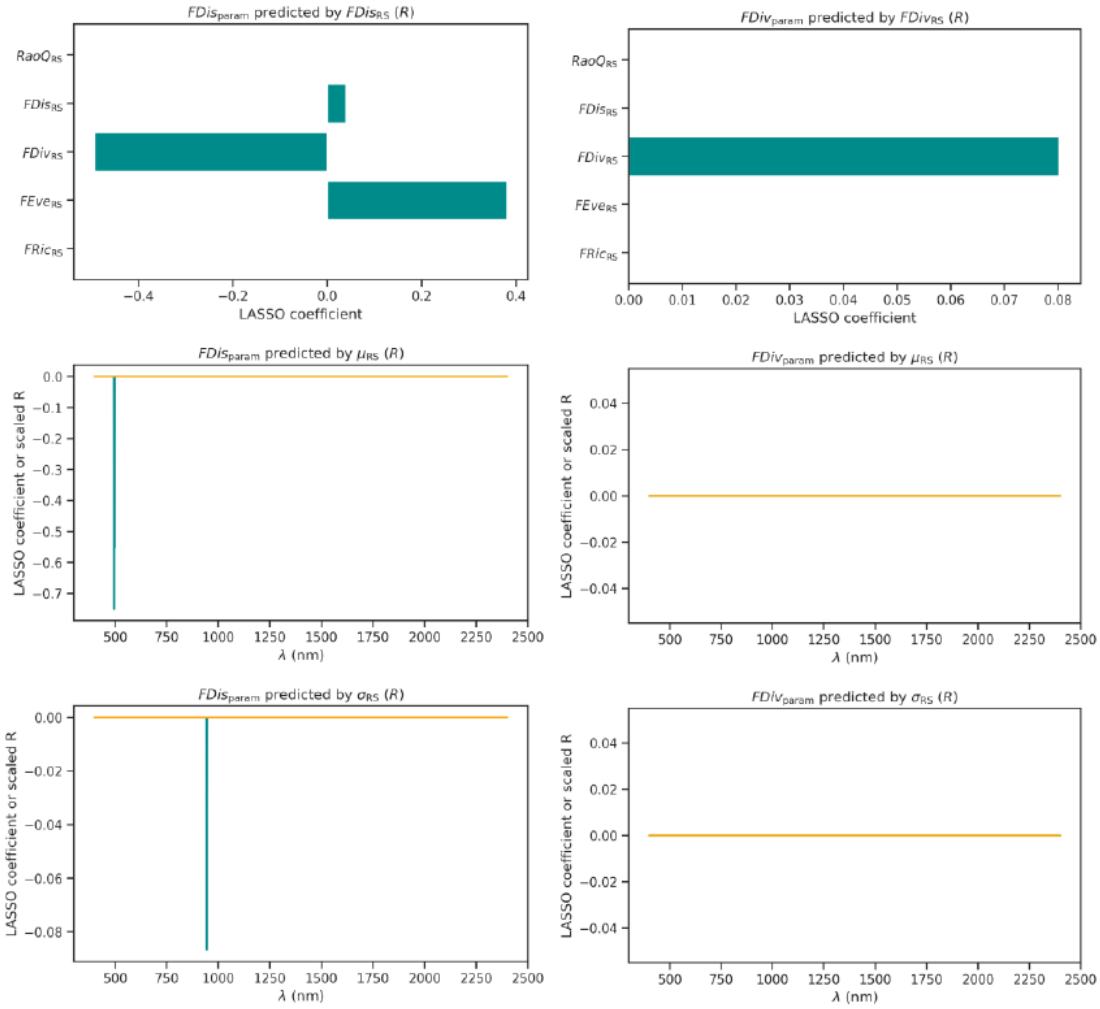

Figure 13. LASSO feature selection to predict biodiversity metrics Functional Dispersion (*FDis*, left) and Functional Divergence (*FDiv*, left) computed from vegetation parameters. Selected features are biodiversity metrics computed from remote sensing data (first row), the weighted average (μ_{RS}, second row), and the standard deviation (μ_{RS}, third row) of the reflectance factors (*R*).

During Y2 and Y2.5, we used more mature simulations to deepen the role of the identity and diversity of the different plant functional traits on spectral diversity. The results of the analyses are described in sections RD1.1.b and RD1.1.c brought additional questions regarding the requirements for evaluating remote sensing estimates of plant functional diversity. Since these might have to cover extensive areas and be stratified by species or plant functional types, it would be important to understand if a reduced set of plant traits with a mechanistic effect on the spectral properties of vegetation could summarize plant functional diversity. This last point is relevant since some functional traits could play marginal roles in light-plant interactions. We repeated simulations but computed FDMs individually for each plant trait to answer this question. Then we analyzed the variance explained by each trait-FDM on the FDMs computed from the complete remote sensing datasets of spectral or optical traits. We used four machine learning models to ensure that results were not determined by the statistical model (Neural Networks, Gaussian Process Regression, Random Forest Regression, and LASSO). For each model, we used

different techniques to assess the role of each plant trait on the remote sensing estimates of plant functional diversity: Global sensitivity analysis, permutation variable importance, and SHAP (SHapley Additive exPlanations). These analyses led to many results (9 FDMs x 3 models x 3 variable importance analyses x 2 remote sensing inputs (spectral and optical traits)) that were coherent with each other. For example, Figure 14 shows how the different variable importance estimates obtained for a Neural Network model fit for $RaoQ_{\alpha=1}$ coherently identify the most relevant plant traits. Similarly, Figure 15 presents the coherence found in permutation variable importance for the four machine learning models trained on $RaoQ_{\alpha=1}$. Like the rest of the FDMs that proved able to link remote sensing and plant functional diversity, results are consistent across models and importance metrics.

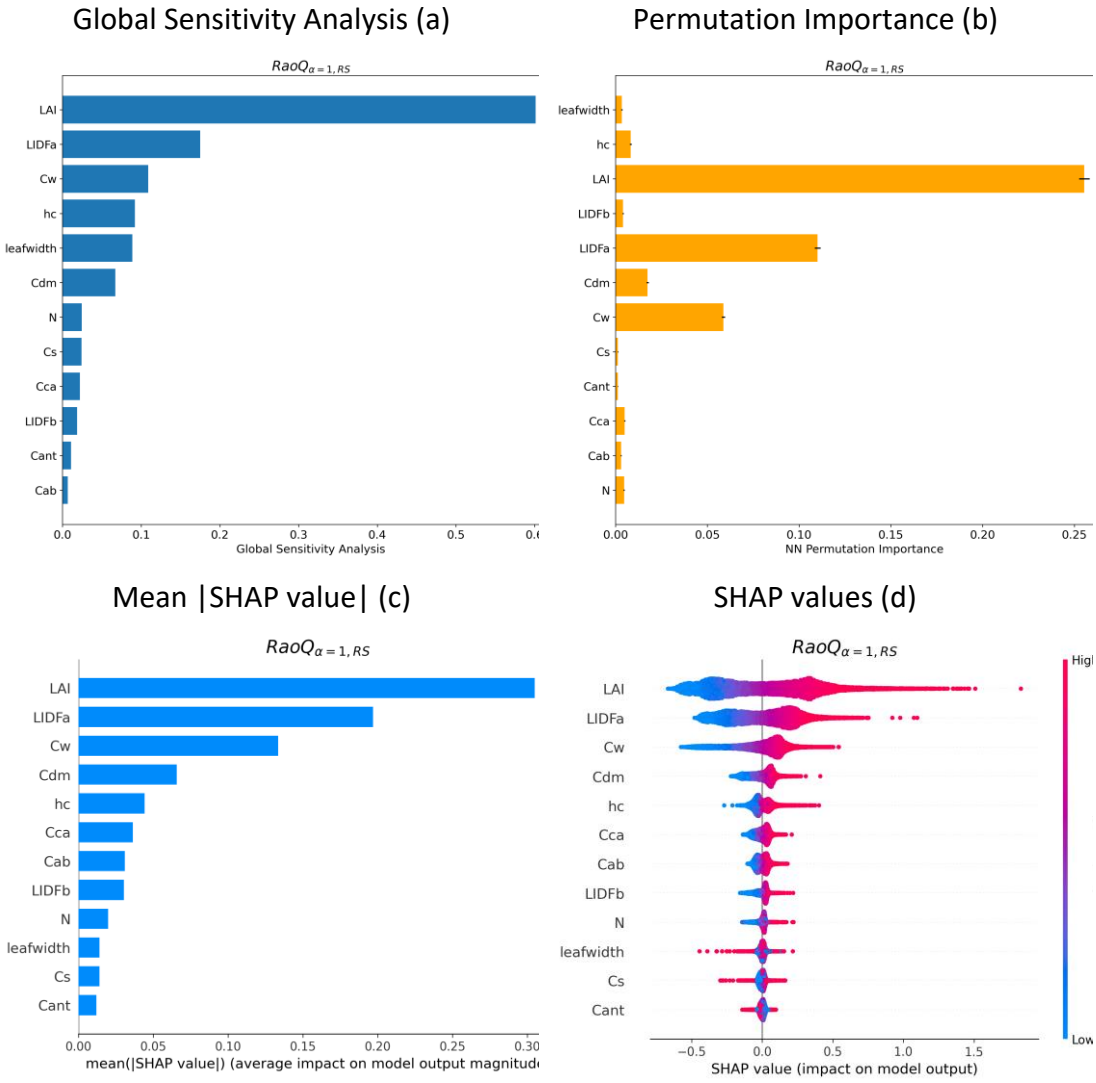

Figure 14. Variable importance metrics computed from the Neural Network model predicting spectral diversity $RaoQ_{\alpha=1}$ from individual plant traits $RaoQ_{\alpha=1}$.

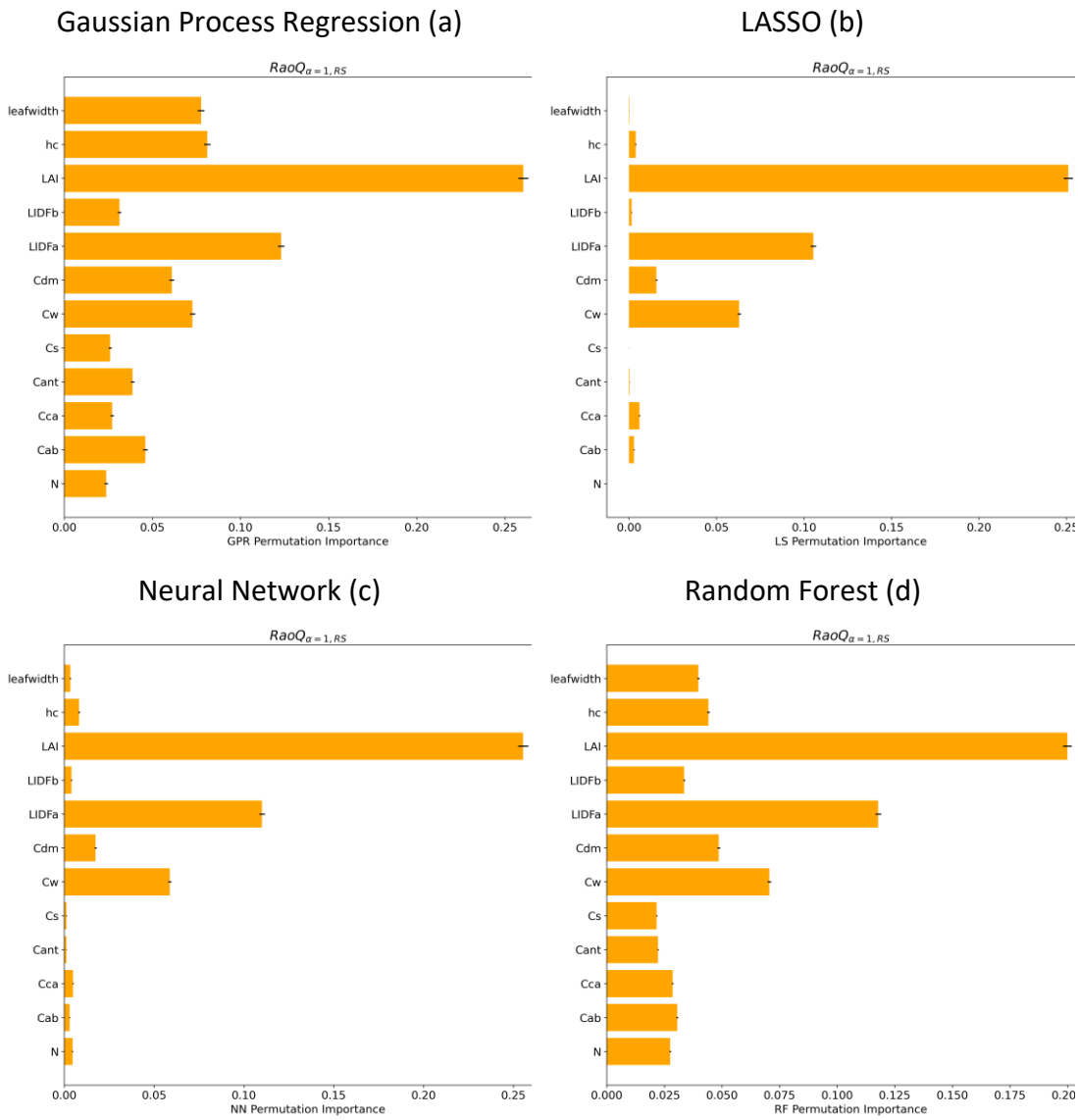

Figure 15. Permutation variable importance for four machine learning models training to explain spectral variability spectral diversity $RaoQ_{\alpha=1}$ from individual plant traits $RaoQ_{\alpha=1}$.

As in the previous analyses (RD1.1.c), we also analyzed the effect of spatial resolution and spectral configuration on relationships between individual plant traits and spectral diversities. Results showed that spatial resolution modifies the relationship between individual traits and remote sensing FDMs (Figure 16), gaining the initially most minor influential parameters some importance. This result was likely a consequence of the explicative power loss of the main traits. As in the previous analyses, the spectral configuration induced lesser differences (mainly between foliar traits) in these relationships in the context of the spectral trait approach (Figure 17). Sentinel-2 resembled more the full-hyperspectral configuration than DESIS, likely because it carries information from the SWIR region.

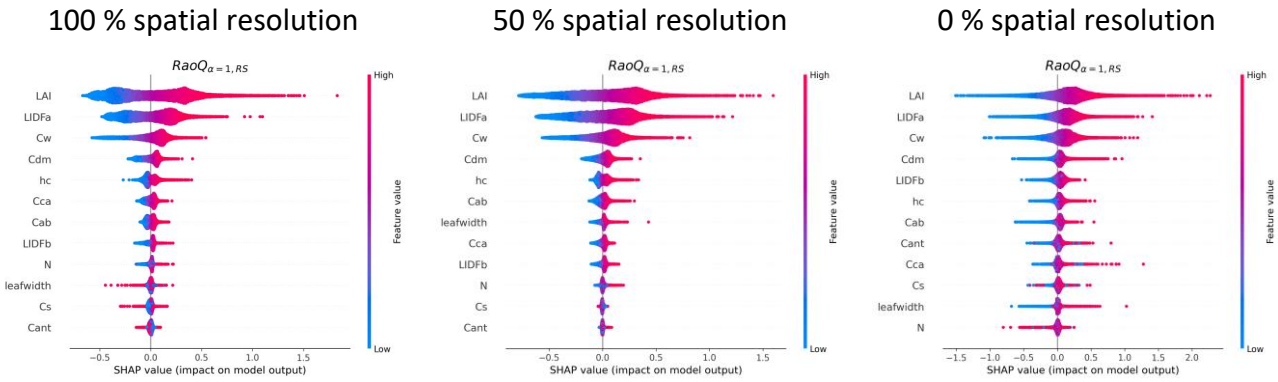

Figure 16. SHAP values for the Neural Network trained to predict spectral diversity *RaoQ*$_{\alpha=1}$ from individual plant traits *RaoQ*$_{\alpha=1}$ matching high spatial resolution field data with full-hyperspectral data at different spatial resolutions.

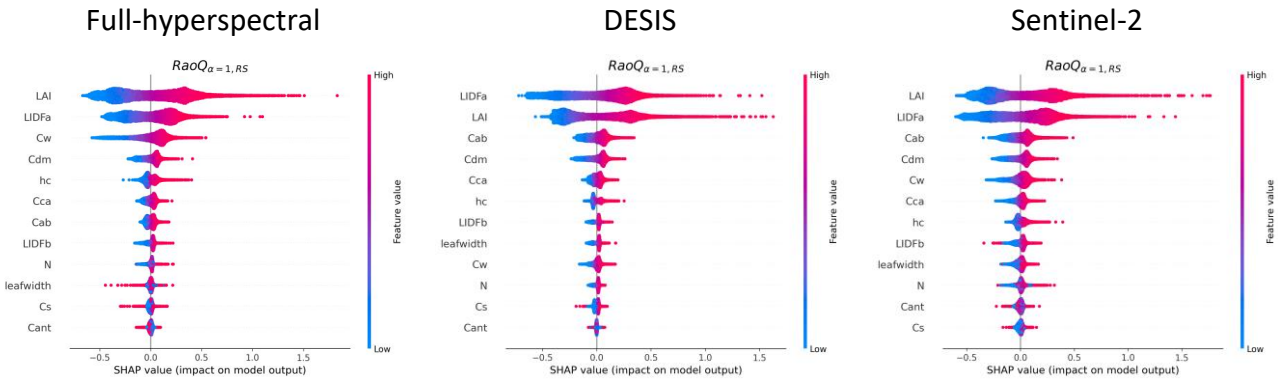

Figure 17. SHAP values for the Neural Network trained to predict spectral diversity *RaoQ*$_{\alpha=1}$ from individual plant traits *RaoQ*$_{\alpha=1}$ at maximal spatial resolution for different spectral configurations.

These analyses led to the following conclusions:

1) The stronger the correlation between field and remote sensing FDMs, the clearer the feature importance differences between variables.
2) Spatial resolution modifies the role played by individual plant traits on plant functional and spectral diversities: suboptimal resolutions dissolve the importance between plant traits but reduce the overall explicative power of the models. In the case of spectral trait approaches, spectral configuration led to minor differences, which are likely controlled by the spectral regions covered by the sensor rather than the specific spectral resolution.
3) Structural parameters (particularly leaf area index (*LAI*) and mean leaf angle inclination (represented by *LIDFa*)) featured a stronger control over

the relationships than foliar traits, among which leaf water content (C_w) and dry matter content (C_{dm}) were the most explicative. While pigments have a strong effect on vegetation optical properties (in particular chlorophyll (C_{ab}) and carotenoids (C_{ca})), their covariance might be responsible for the reduced importance they were individually assigned.

These relevant results stress the gap between remote sensing and ecology communities. Whereas ecological studies of plant functional diversity focus on foliar traits as descriptors of the variability of functions, our results give a predominant role to structural traits controlling light-plant interception. Further research is clearly needed in this direction; efforts should focus on linking the information contained in spectral signals with the information sought by ecologists, who would interpret and use future maps of plant functional diversity generated by remote sensing.

During Y2 and Y2.5, we worked on emulating more complex radiative transfer models, such as FLIGHT (RD1.1.a), to quantify the effect of additional structural factors and bare soil. However, its emulation was not satisfactory enough, and the analyses performed were not considered reliable to cast strong conclusions as presented above.

RD1.1.e. Global normalization of functional diversity metrics and diversity partitioning at different spatial scales.

Biodiversity analysis is dependent on the scale. In Y2, we extended the use of the simulation framework to assess methods partitioning biodiversity into the classical alpha (α), beta (β), and gamma (γ) components. These represent the average diversity of an area (α), the diversity turnover between different areas (β), and the total diversity of the region composed of those areas (γ). Literature research presented two possible approaches, one based on variance analysis that had been recently proposed in the context of remote sensing (Laliberté et al. 2020) and diversity partitioning based on Rao's *Q* index and concretely in its equivalent number (de Bello et al. 2010). The equivalent number is a transformed version of the index that provides index-formulation independent variables with mathematical properties able to provide unbiased estimates of β-diversity (Jost 2006, 2007). This bias is a consequence of the fact that β-diversity is often calculated as a function of the relationship between α and γ-diversities; and is more pronounced when α-diversity is high. However, neither Rao *Q* nor equivalent numbers have been yet used in remote sensing to partition biodiversity spatial components.

The calculation of equivalent numbers led to a new challenge arising from the limited size of the datasets used by ecologists in comparison with the evergrowing remote sensing data and the fact that the second aim at producing comparable estimates. The calculation of equivalent numbers requires normalizing the dissimilarity metric (i.e., the Euclidean distance of the principal components summarizing the information in the trait space). While this is done using the maximum dissimilarity value in ecological studies, it is not feasible in the remote sensing context. Even more, we proved that this normalization, when applied image per image, makes the values of the different diversity estimates not comparable between datasets;

which is a problem for generating global biodiversity products. The solution to this problem led to a new global normalization approach applicable to several FDMs and biodiversity component estimates. Global normalization solves the issue that the diversity metrics value depends on the dataset analyzed's dimensionality. For example, in remote sensing, sensors featuring different numbers of spectral bands would produce different values even if they carried the same information regarding plant functional diversity (which simulations show is plausible due to the high autocorrelation of spectral reflectance). The normalization approach exploits two ideas regarding standardization and principal component analysis that precedes the computation of FDMs. First, it is possible to describe maximum and minimum bounds in the standardized space as a function of the dataset's standard deviation. Second, in a context where traits can be bounded within plausible ranges of variation, the maximum dissimilarity would only be provided by fully decorrelated datasets. From these premises, we developed different formulations to standardize Rao *Q*, *FRic*, and the biodiversity α, β, and γ components calculated either with variance analysis or with equivalent numbers.

The global normalization approach provides metrics that are directly comparable (in the 1:1 regression line) as long as they carry the same diversity information, independently of the set of traits with which these are generated. The consequences of this are of maximum relevance:

1) Functional diversity estimates from different remote sensing missions can be directly combined or compared to generate dense time series, gap-fill cloud coverage, or assess their performance against field data directly.
2) The fact that normalization should bring the same information content to the 1:1 line provides a reference for comparing FDMs estimated from different missions or field datasets. Normalized metrics make it possible to understand if a particular mission or metric over or underestimates the estimates obtained from field samples or missions with different spectral and spatial features.
3) Heterogeneous field datasets can be integrated to validate remote sensing products of plant functional diversity.

This is a very important contribution, not only in the context of remote sensing but also in the context of ecology, not initially foreseen in the project. The approach was submitted in June 2022 to Methods in Ecology and Evolution. The journal answered with a positive review in November 2022. In addition, we have produced a Python package to apply global normalization to the computation of different FDMs and diversity partitioning methods.

The development of this method led as well to a new collaboration that has strengthened links between ecology and remote sensing communities; specifically, we contacted Dr. Francesco de Bello, from the Spanish National Research Council. Dr. De Bello is an expert in functional diversity metrics who pioneered using Rao's *Q* and its equivalent number to partition diversity components. He helped to understand the problems found in the first analyses involving equivalent numbers and to adapt the simulation framework to make simulations more realistic.

The advantages of the global normalization approach were evaluated using an adapted simulation framework (RD1.1.a) that again provided full control and understanding of the relationships to be analyzed. Figure 18 summarizes the analyses performed. As can be seen, different FDMs and diversity partitioning methods were assessed, either applying no normalization, image-based normalization (this is, using the maximum dissimilarity found in a single image or region), and the global normalization proposed by oBEF-Accoss2. Then, different statistics were used to assess to what extent each normalization approach placed the metrics in a directly comparable scale (1:1) and the strength of the correlation.

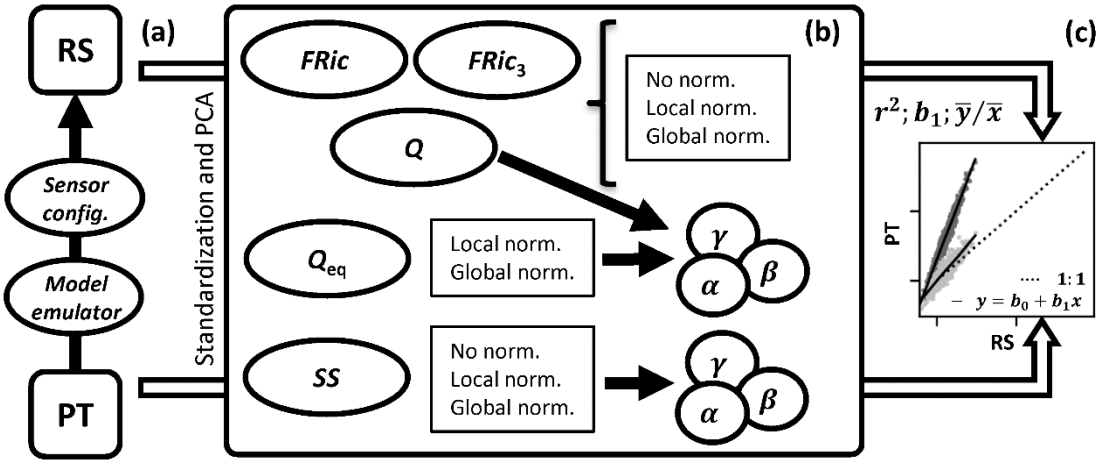

Figure 18. Workflow summary. First, a radiative transfer model emulator uses plant traits (PT) featuring species of simulated communities to predict remote sensing (RS) variables (i.e., reflectance factors), which are resampled to the spectral features of different remote sensors (a). Second, PT and RS variables are transformed (standardization and dimensionality reduction with principal component analysis (PCA) and used to compute different functional diversity indices (functional richness and Rao's *Q* entropy), Rao's *Q* equivalent number (Q_{eq}), and the sum of squares (*SS*). These undergo different normalizations (none, local, global). Then, Rao's and *SS* metrics are used to partition α, γ, and γ-diversity components (b). Third, the relationships between metrics and diversity components estimated from RS or PT variables are evaluated using the Pearson correlation coefficient, the slope of the linear model, and the average ratio (c).

Figure 19 shows how different normalizations affect the comparability of FDMs computed from a full hyperspectral sensor and field plant traits. *FRic* of datasets of large dimensionality can be computationally demanding since it requires calculating the convex-hull volume in a multidimensional space. Therefore, we limited the calculation of *FRic* over a maximum of 8 PCA selected from the spectral or plant trait datasets (*FRic*). In addition, we computed a second version where the maximum number of PC was 3, which is often used in ecology and remote sensing studies ($FRic_3$). We also tested the normalization on Rao *Q* and its equivalent number (Q_{eq}). As shown in the first row, when no normalization is applied, the magnitude of the metrics strongly depends on the dataset dimensionality. Remote sensing and plant trait FDMs show differences of orders of magnitude. Image-based normalization only improves for *FRic*, whereas it decreases for $FRic_3$, Rao *Q*, and Q_{eq}, whereas it does not achieve dimensionality-independent values. Global normalization shows the same correlation as the non-normalized Rao *Q* and Q_{eq} while placing them on the same scale. It also improves the correlations for *FRic* and $FRic_3$ but fails to set them on the same scale.

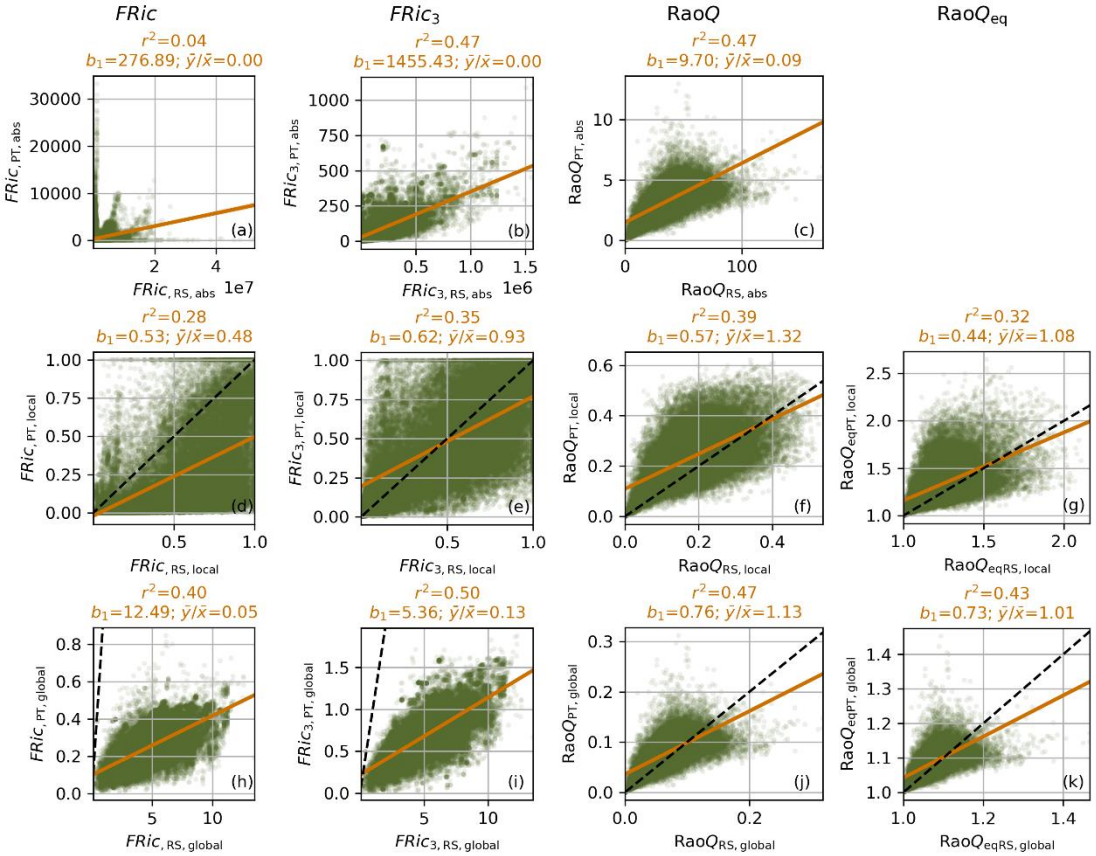

Figure 19. Diversity indices and equivalent numbers computed without (first row), with local (second row), and with global normalization (third row) corresponding to field plant trait (*y*-axis) and full-hyperspectral remote sensing (*x*-axis) datasets. *FRic* (first column), *FRic* limited to up to 3 principal components (second column), Rao *Q* index (third column), and its equivalent number (fourth column). Pearson correlation coefficient (r^2), the linear model slope (b_1), and the averages' ratio ($\bar{y}/\bar{x}$) are presented.

The results are coherent for different spectral configurations (Figure 20). In all cases, global normalization performs better than image-based normalization. It keeps or improves the correlations between remote sensing and field plant trait FDMs, whereas it gets their values closer to the same scale, particularly for *RaoQ* and Q_{eq}. Consequently, remote sensing metrics are not only more comparable among each other but also with field datasets.

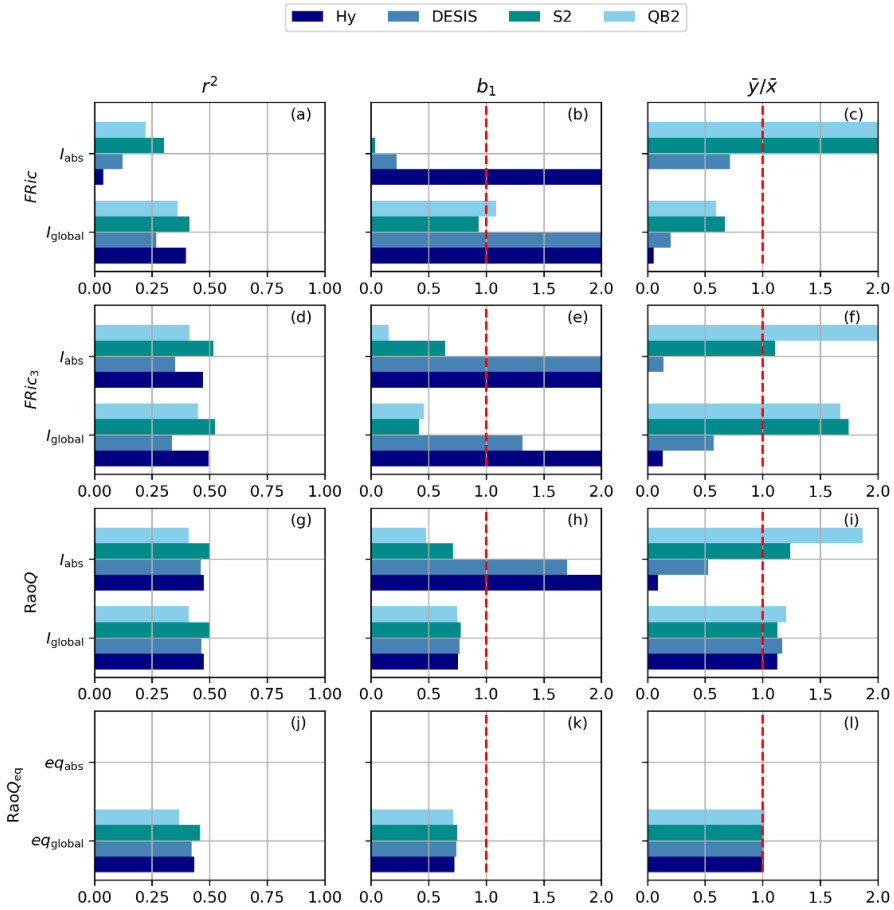

Figure 20.

Comparison of absolute and globally-normalized diversity metrics for different remote sensors: Full-hyperspectral (Hy), DESIS, Sentinel-2 (S2), and Quick Bird 2 (QB2). Pearson correlation coefficient (r^2), the linear model slope (b_1), and the averages' ratio ($\bar{y}/\bar{x}$) are presented; the red dashed line indicates unity. *FRic* (first column), *FRic* limited to up to 3 principal components (second column), and Rao *Q* (third column) and its equivalent number (fourth column).

Global normalization also proved helpful for the different diversity partitioning methods. Figure 21 shows the diversity decomposition results based on *RaoQ* and its equivalent number Q_{eq} and compares the metrics obtained from hyperspectral data and field traits. Compared to the not-normalized approach (first row), global normalization (third row) on *RaoQ* is more comparable and strongly correlated than image-based normalization (second row). In these cases, the fraction of α and β-diversity over γ-diversity (f_α and f_β, respectively) does not change. Results are similar for Q_{eq}; however, image-normalization leads to biased fractions f_α and f_β; whereas global normalization compresses their ranges of variation, which is coherent with the definition of equivalent number when a large number of functional traits is analyzed. Still, the degree of usefulness of the partitions performed using *RaoQ* or Q_{eq} should be determined by the ecologists, who are the community targeted for exploiting the new remote sensing products. As before (Figure 20), global normalization makes comparable the FDMs computed from different RS missions (not shown), which is of maximum interest for analyzing diversity maps produced from various data sources.

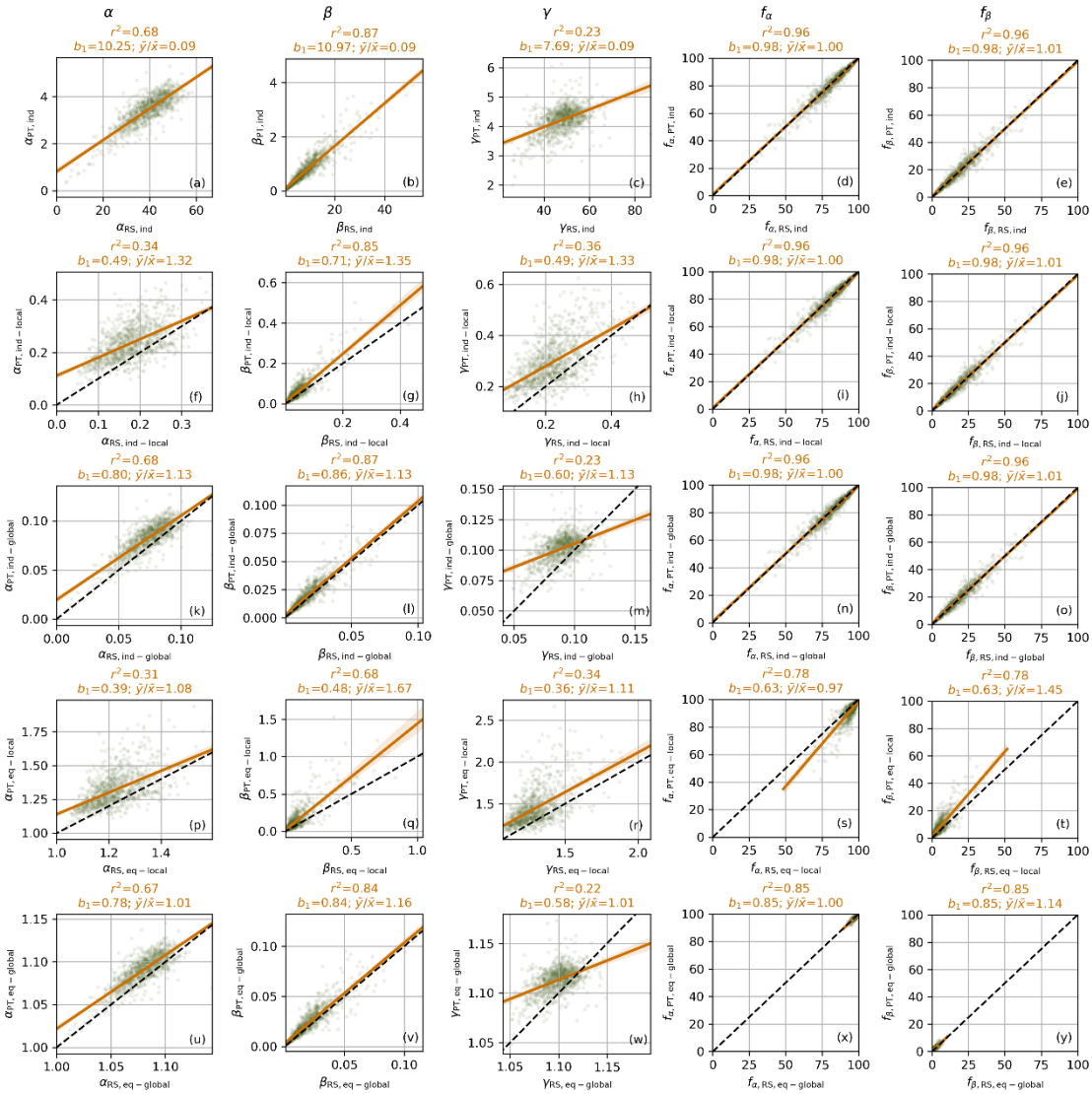

Figure 21. Diversity decomposition using the diversity index Rao *Q* without (first row), local Rao *Q* (second row), and global normalization Rao *Q* (third row), or its equivalent number with local (fourth row), and global normalization (fifth row) corresponding to field plant trait (*y*-axis) and full-hyperspectral remote sensing (*x*-axis) datasets. Estimates of α (first column), β (second column), and γ (third column) diversity, as well as the fractions of α (fourth column) and β (fifth column). Pearson correlation coefficient (r^2), the linear model slope (b_1), and the averages' ratio ($\bar{y}/\bar{x}$) are presented.

Global normalization also offers advantages for variance-based partitioning methods (Figure 22). This method captures γ-diversity better than the previous one, based on *RaoQ* (Figure 21). Also, it improves the correlation between field and remote sensing estimates, whereas the fractions remain unaltered and less precise. However, as before, image-based normalization proves not to be a recommendable method in the context of remote sensing.

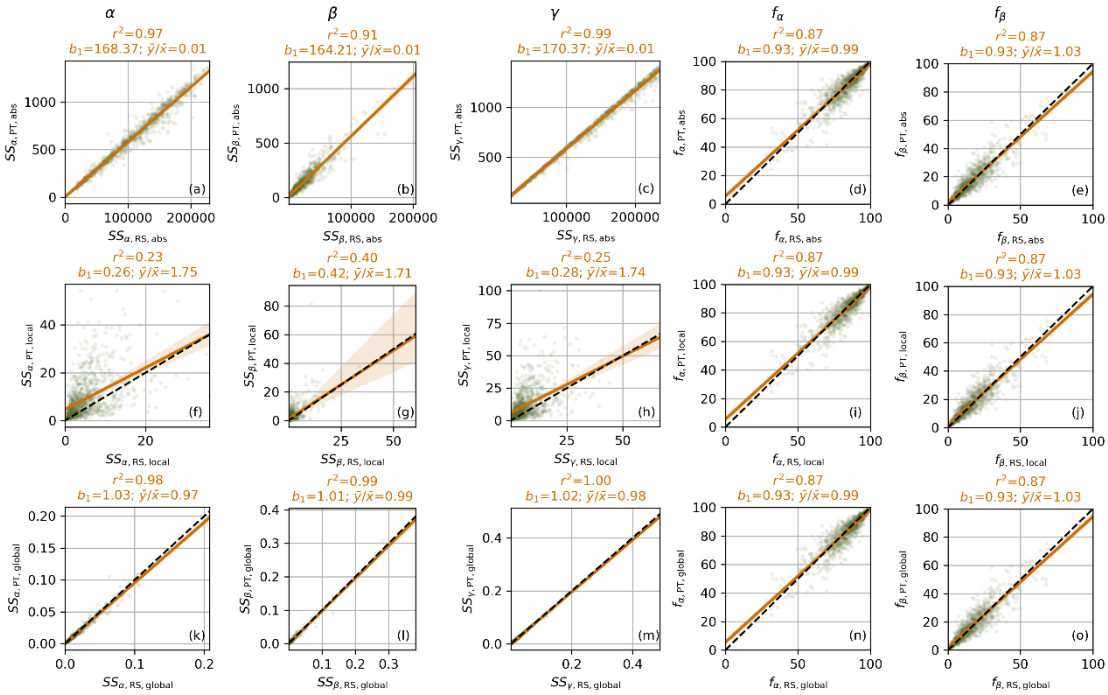

Figure 22. Diversity decomposition using variance without (first row), with local (second row), and global normalization (third row) corresponding to field plant trait (*y*-axis) and full-hyperspectral remote sensing (*x*-axis) datasets. Estimates of α (first column), β (second column), and γ (third column) components, as well as the fractions of α (fourth column) and β (fifth column). Pearson correlation coefficient (r^2), the linear model slope (b_1), and the averages' ratio ($\bar{y}/\bar{x}$) are presented.

The capability of global normalization to place diversity estimates at the same scale is evident in Figure 23, which compares the non-normalized with the global normalization values. Thanks to this new approach, the differences in spatial resolution will dominate the estimates of different missions, enabling analyzing scale effects directly with observational data. This oBEF-Accross2 unexpected contribution is of maximum relevance; it solves one of the major limitations in interpreting diversity estimates obtained from different sensors and enables direct comparison of metrics computed from the field or remote sensing datasets. The computation of normalized metrics, both for *FRic*, *RaoQ*, or *Qeq*, and the two diversity partitioning methods described above have been implemented in a python package that will be released with the publication currently under review in Methods in Ecology and Evolution.

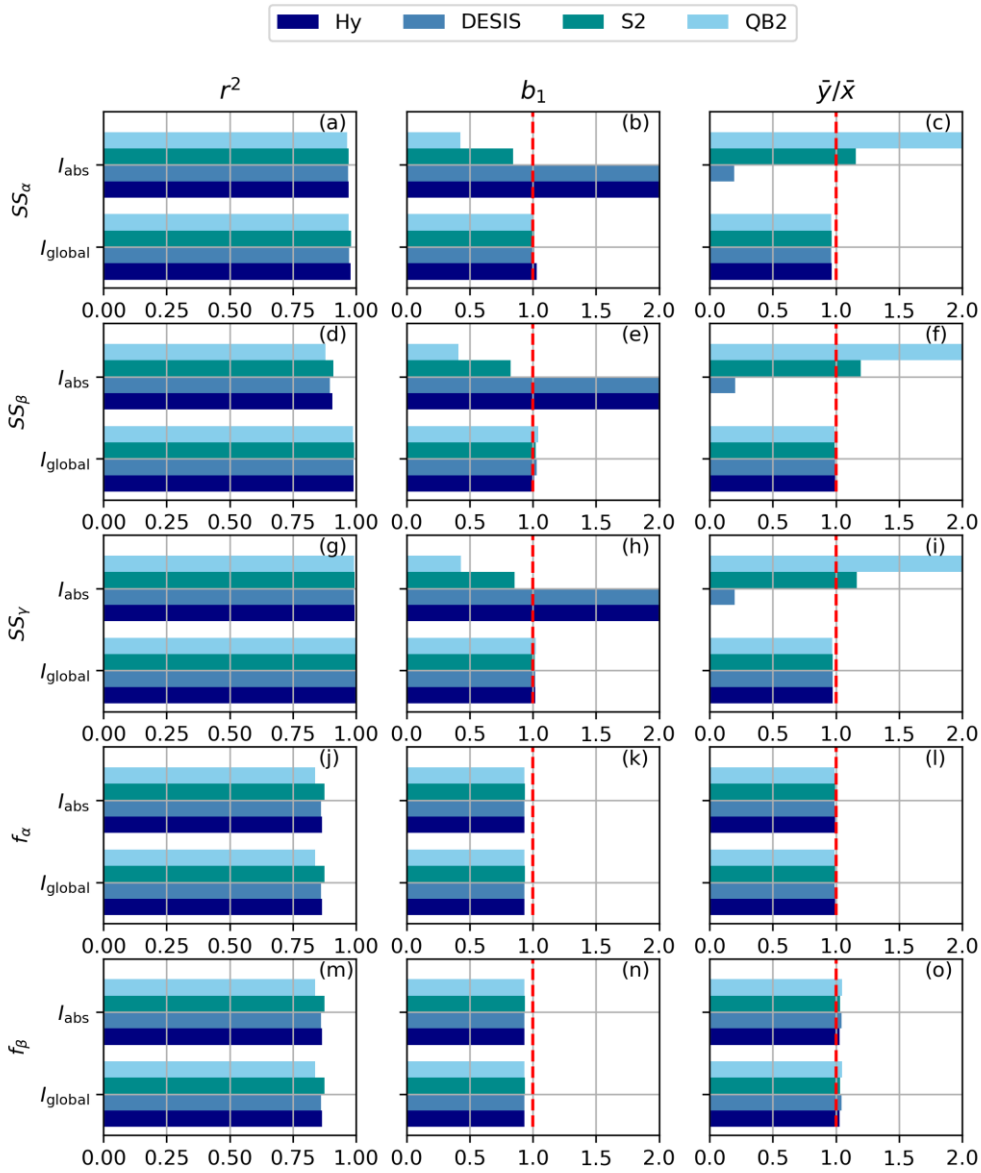

Figure 23. Comparison of the variance-based diversity decomposition without and with global normalization: Full-hyperspectral (Hy), DESIS, Sentinel-2 (S2), and Quick Bird 2 (QB2). Pearson correlation coefficient (r^2), the linear model slope (b_1), and the averages' ratio ($\bar{y}/\bar{x}$) are presented; the red dashed line indicates unity. Estimates of α (first row), β (second row), and γ (third row) components, as well as the fractions of α (fourth row) and β (fifth row).

RD1.1.f. Quantifying functional diversity with airborne remote sensing imagery – A case study on the potential of sun-induced chlorophyll fluorescence.

oBEF-Accros2 also went beyond simulation in exploiting spectral signals linked to plant photosynthesis. In collaboration with the University of Milano-Bicocca (Italy) and the University of Extremadura (Spain), we analyzed the effects of fertilization on plant functional diversity using Hyplant imagery acquired over the study site of Majadas de Tiétar in Spain. This ecosystem station monitors the responses of a Mediterranean woody savanna to a large-scale manipulation experiment with Nitrogen and Phosphorus (MANIP) using remote and three sets of eddy-covariance towers. The experiment took place over three areas of 200 x 400 m; one of them was the control (CT), and the other two were fertilized with Nitrogen (NT) and with Nitrogen plus Phosphorus (NPT) (Figure 24). In July 2018, the site was imaged by Hyplant, a hyperspectral system comprehending a VSIWR sensor and a specific sensor designed to retrieve sun-induced chlorophyll fluorescence (SIF). SIF is an emission related to the electron transport rate of photosynthesis and regulated by non-photochemical quenching.

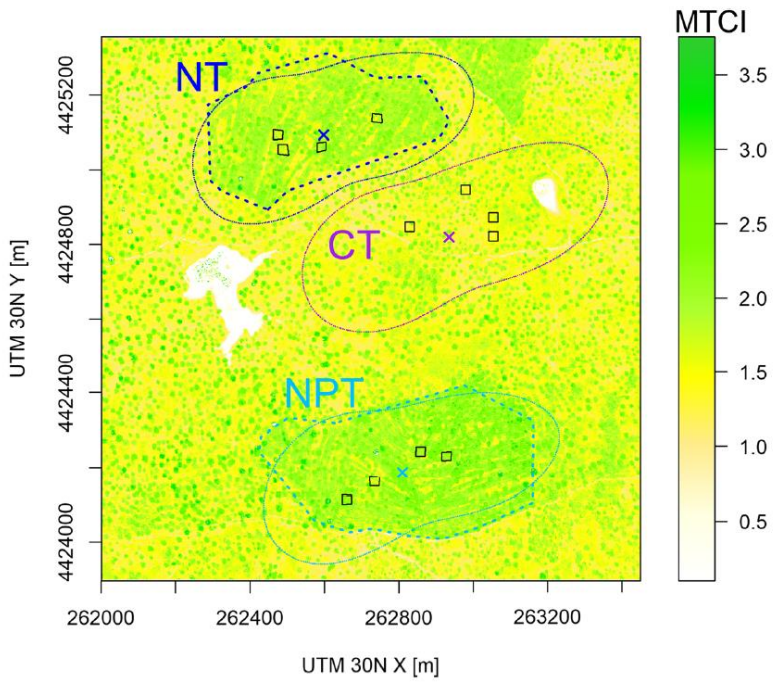

Figure 24. Post-fertilization MERIS Terrestrial Chlorophyll Index (MTCI, a vegetation index associated with the chlorophyll content of vegetation) values from hyperspectral airborne CASI imagery of the study site. Tower locations are indicated with a cross in the center of the respective footprint climatology (80% isolines). The purple symbols represent the control (CT), dark blue the nitrogen (NT), and light blue the nitrogen + phosphorus (NPT) treatment. The dashed lines mark the outer limits of the fertilized areas.

During Y1, we evaluated the relationships between FDMs computed from plant functional traits sampled from 18 grass plots and the colocated reflectance and sun-induced chlorophyll fluorescence airborne imagery. Specifically, we assessed the Normalized Difference Vegetation Index (*NDVI*) and fluorescence radiance retrieved in the O_2-A band (760 nm, F_{760}). However, only part of the plant traits sampled directly

influenced light-plant interaction (i.e., canopy height or specific leaf area). The rest either had an indirect effect due to their presence in absorbing molecules (such as nitrogen concentration) or barely affected the spectral signals and instead related with plant function (i.e., isotopic 13C discrimination specific root length and root tissue density). To gain more mechanistic insight into these relationships, oBEF-Accross2 contributed to these analyses by estimating optical traits (some of them Essential Biodiversity Variables) and performing simulations. These simulations helped to understand the interlinks between the diversity of spectral signals (*NDVI* and F_{760}) and the diversity of the potential drivers such as photosynthetically active radiation absorbed by chlorophyll ($aPAR_{Chl}$), fluorescence scape probability at 760 nm ($F_{esc,760}$), and fluorescence yield at 760 nm ($F_{yield,760}$). We initially estimated the optical traits inverting a primitive version of senSCOPE (Pacheco-Labrador et al. 2020b), a modification of the model SCOPE adapted to Mediterranean grasslands featuring mixtures of green and senescent plants such as the study area. During Y2, these analyses were enhanced with the consolidated version of senSCOPE (Pacheco-Labrador et al. 2021a), which included new specific absorption coefficients of senescent pigments. Moreover, we used the emulator described in R1.1.a to speed up the analyses.

In Y1, our colleagues found stronger correlations for F_{760} than *NDVI* diversity with field FDMs. However, simulation analyses carried out in the context of oBEF-Across2 (RD1.1.b) revealed that it was necessary to apply standardization and PCA dimensionality reduction before computing FDMs to allow the correlation between field plant and spectral traits. Standardization had not been applied to the field trait datasets in the first analyses. In Y2, our colleagues corrected their processing and found no significant relationships between field plant functional diversity and spectral diversity from *NDVI* or F_{760}. While this was bad news for the undergoing research, detecting and correcting this methodological problem was essential. We further tested different optical trait retrieval approaches to reproduce and better understand the observational results without success. While unclear, we concluded that the lack of correlation might be related to suboptimal spatial resolution or the lack of influence of some of the plant traits on the spectral signals. Still, our simulations contributed to understanding the drivers of the spatial variability of F_{760} than *NDVI*. As shown in Figure 25, *RaoQ* calculated on the pixel $aPAR_{Chl}$ explains most of the NDVI *RaoQ* variance, whereas $F_{yield,760}$ explains most of the F_{760} *RaoQ* variability. This indicates a higher F_{760} sensitivity to physiological than structural information. These results were presented at the World Biodiversity Forum in Davos in June 2022 (Tagliabue et al. 2022). After realizing the limitations of the field datasets to validate the diversity estimates obtained from airborne imagery, our colleagues reoriented their efforts to assess the role of tree crowns on the grassland's functional diversity. They tested the hypothesis that trees reduce environmental filtering and enable larger diversity. Results from field samples and imagery confirmed this hypothesis, whereas spatial resolution limited the analyses since facilitation is the strongest in the closest area around the trees, which was often removed from imagery to prevent tree crowns from affecting the metrics.

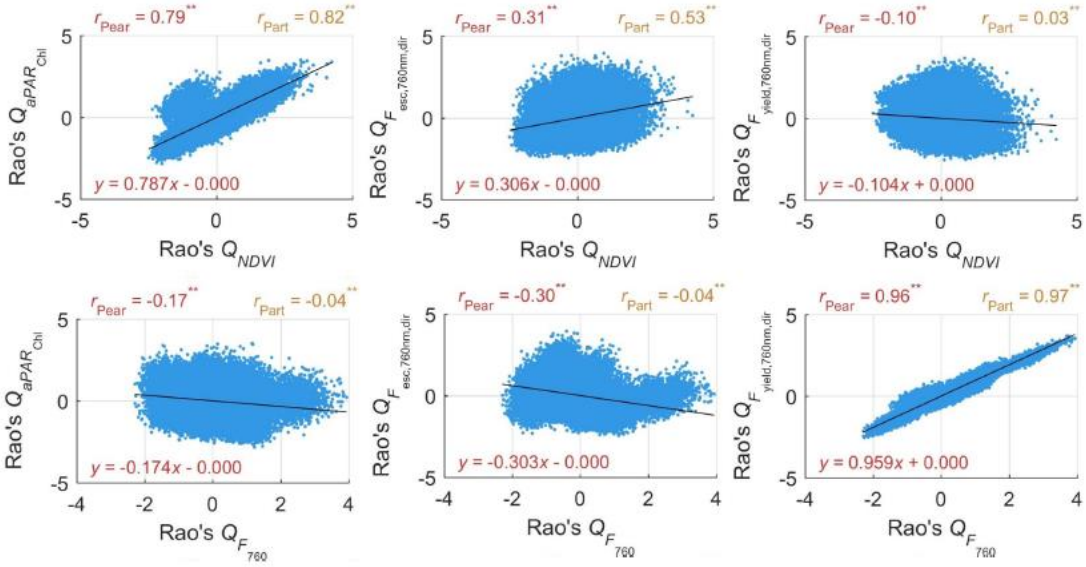

Figure 25. Linear regression between Rao Q computed from the Normalized Difference Vegetation Index (*NDVI*) and sun-induced chlorophyll fluorescence radiance at 760 nm (F_{760}) with the photosynthetically active radiation absorbed by chlorophyll ($aPAR_{Chl}$), fluorescence scape probability at 760 nm ($F_{esc,760}$), and fluorescence yield at 760 nm ($F_{yield,760}$). The plots show the Pearson correlation coefficient and the partial correlation coefficient. In addition, ANCOVA analysis supported these results.

We also attempted to improve the functional diversity mapping using airborne hyperspectral imagery to retrieve biophysical and physiological variables (optical traits, some Essential Biodiversity Variables) during Y1. The reason for this was overcoming the presence of shades in the optical imagery by exploiting the trait estimates directly. Previous attempts had not been satisfactory enough for publication (Pacheco-Labrador et al. 2020a), partly due to the inability of 1D radiative transfer models to represent Mediterranean woody savannas. To improve this representation, we combined senSCOPE with a geometrical/optical model simulating tree crowns and their shades over the grassland. In addition, we used the ECOSTRESS spectral library to improve the representation of soil and vegetation thermal properties. Also, we trained machine-learning models over look-up tables to accelerate data assimilation. While these efforts improved the retrieval of vegetation properties and fluxes, we still found large uncertainties in estimating some plant functional traits. Therefore, we prioritized other analyses of higher scientific interest with more potential for achieving the project's objectives.

RD1.2: Biodiversity prediction based on spectral, structural, and phenological information

During Y1, we focused on analyzing hyperspectral DESIS imagery provided over the FunDivEUROPE sites by the "Data Announcement of Opportunity" *EBioIDEA: Enhancing Biodiversity Inventories with DESIS Imagery Analysis* (Figure 26). First, we used DESIS data to compare the information contained in hyperspectral or multispectral datasets (Figure 1). Here, we also increased and tested the range of

FDMs initially foreseen, including a parametric version of *RaoQ* from Rocchini et al. (2021). Moreover, in Y2, we compared it with Sentinel-2 to evaluate the simulation framework (RD1.1.c, Figure 11, and Figure 12).

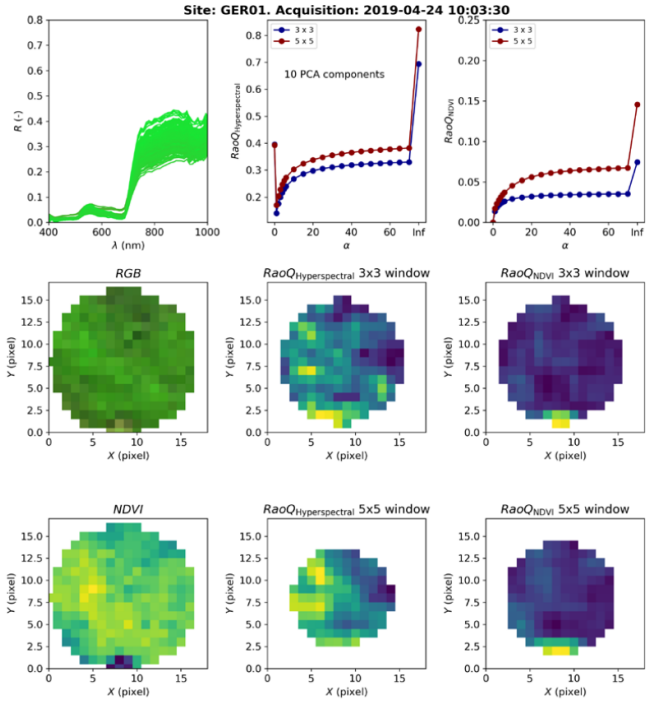

Figure 26. Functional diversity maps and metrics computed from DESIS imagery acquired on the FunDivEUROPE site GER01. The first column shows the spectral reflectance factors, an RGB, and *NDVI* map corresponding to a cut-out of a 250 m radius around the site. The second column presents Rocchini et al. (2021) Rao's Q metric and maps computed from the hyperspectral data for different moving window sizes. Finally, the third column shows similar results computed from NDVI.

The conclusions provided by the simulation and related observational analyses (RD1.1a-d) led us to focus on using Sentinel-2 data to tackle RD1.2. On the one side, RD1.1 showed that hyperspectral and multispectral traits similarly capture plant functional diversity if spatial resolution is adequate. On the other side, the noisy nature of this data could limit its applicability for using FDMs since RADAR speckle could spuriously inflate their values. We discussed this specific problem in Pacheco-Labrador et al. (2022b). Furthermore, during Y2, we found challenges in interpreting functional diversity's temporal variability. Therefore, during Y2.5, we tried to improve the time series construction to reduce noise and the influence of data gaps (e.g., clouds) to facilitate the interpretation of phenological diversity. In addition, we used the new global normalization approach developed in RD1.1.d.

During Y2, we analyzed spectral diversity in FunDivEUROPE plots. The first analyses focused on the spatial extent and showed that it influences FDMs, thus recommending comparing areas of similar size. However, the way plot surface and FDM relate changes between different plant communities. Figure 27 shows the variability in the average $RaoQ_{\alpha=1}$ in circular areas with different *radii* around plots of three regions of the FunDivEUROPE network. $RaoQ_{\alpha=1}$ decreases with the *radii* in Spain, whereas it increases in Romania and Finland. These results are relevant and

open new questions about the requirements for comparing remote sensing estimates of plant functional diversity from different sites of variable size.

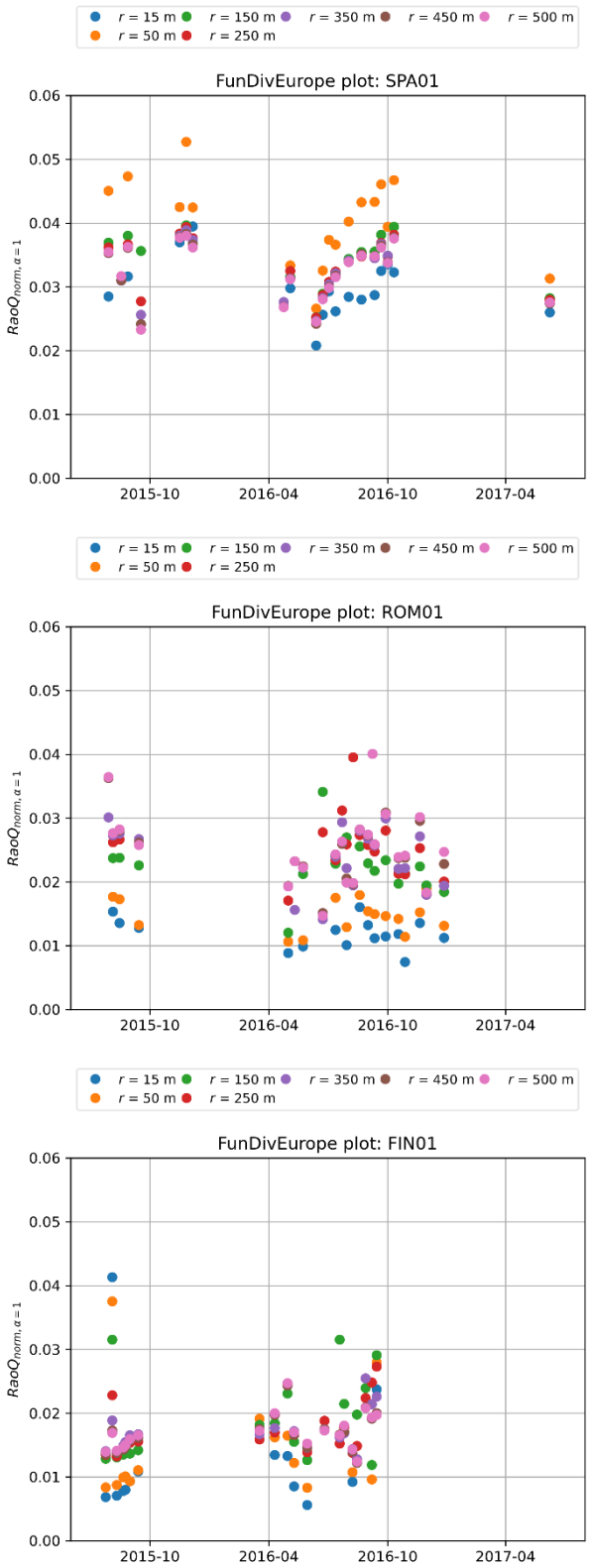

Figure 27. Average $RaoQ_{\alpha=1}$ normalized using the global approach (Pacheco-Labrador et al. under review) in circular areas of varying radii (*r*) centered on plots of the FunDivEUROPE network in Spain (top), Romania (center), and Finland (bottom).

The temporal analysis of individual plots suggested some phenological diversity patterns. For example, in Spain, spectral diversity seems to increase from Spring to Autumn, whereas in Romania, it decreases for the same period. The trend in the Finland plot is not clear (Figure 27). However, these patterns become noisy when all the FunDivEUROPE plots are considered (Figure 28). Part of this noise could be due to the apparition of clouds, cloud shades, and snow or perturbations not necessarily related to vegetation phenology. While the effect of the perturbations cannot be directly corrected, we tested different approaches to minimize the impact of clouds and shades during Y2.5. On one side, we tried to interpolate missing pixels due to clouds, cloud shades, and snow. We performed temporal interpolation of the reflectance factors before computing the different FDMs. On the other hand, we produced monthly composites of the reflectance factors (averages) before calculating the FDMs.

Figure 29 compares the time series of normalized $RaoQ_{\alpha=1}$ obtained using the different correction methods. As can be seen, interpolation only induces slight variations and removes some outliers. Meanwhile, it is unclear the role of interpolation uncertainties in the computation of the metrics. $RaoQ_{\alpha=1}$ on monthly averages of reflectance factors seem to remove some of the time series noise, showing a more apparent increase of spectral diversity from spring to autumn in 2016. Still, the interpretation of the phenological variability of spectral diversity remains challenging. To improve our understanding of this variability and how it could be informative for biodiversity mapping, we compared spectral diversity with ecosystem phenology represented by different spectral indices. Figure 30 presents an example of these relationships with the Normalized Difference Vegetation Index (*NDVI*) for the plots of three regions of the FunDivEurope network. Results were unclear; as can be seen, most of the correlations found were not significant (dashed lines in Figure 30), whereas significant correlations (solid lines in Figure 30) of opposite signs appeared in the same region. Overall, FunDivEurope regions behaved differently. For example, in Spain and Romania, *NDVI* seems more often positively correlated with spectral diversity. In contrast, in Finland, the correlation was negative when significant. *NDVI* relates to the amount of green biomass in the pixel. These results suggest that spectral diversity might increase with biomass in deciduous environments and decrease in evergreen ones. Still, this hypothesis requires deeper analysis and more solid confirmations. We also found discrepancies between and within regions for other commonly used spectral indexes computed from Sentinel-2, which did not always support this idea (e.g., the MERIS Terrestrial Chlorophyll Index presented large region variability and unclear trends). Results suggest that spectral diversity (proxy of plant functional diversity) is not necessarily related to vegetation phenology and might preset different trends for different vegetation types. Still, understanding these relationships demands a better comprehension of the effects of various artifacts, such as background or shades, in the phenological variability of spectral diversity.

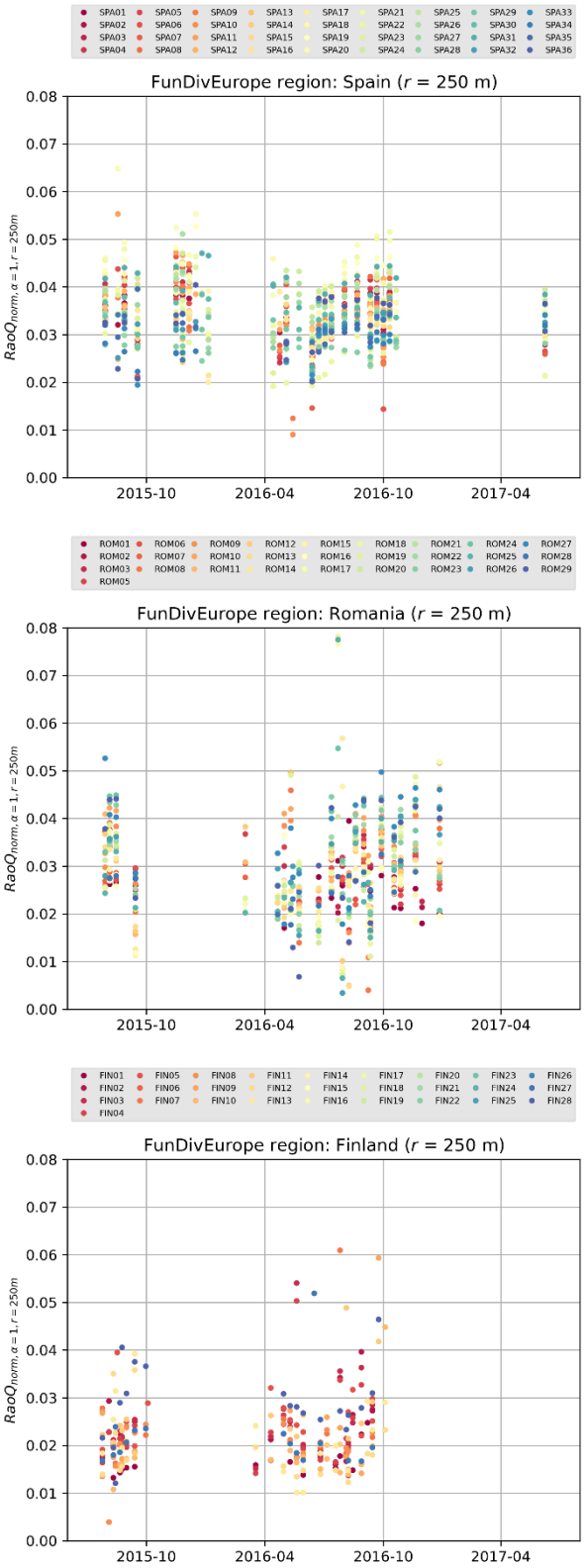

Figure 28. Average $RaoQ_{\alpha=1}$ normalized using the global approach (Pacheco-Labrador et al. under review) in circular areas of 250 m radius centered on the plots of the FunDivEUROPE network in Spain (top), Romania (center) and Finland (bottom).

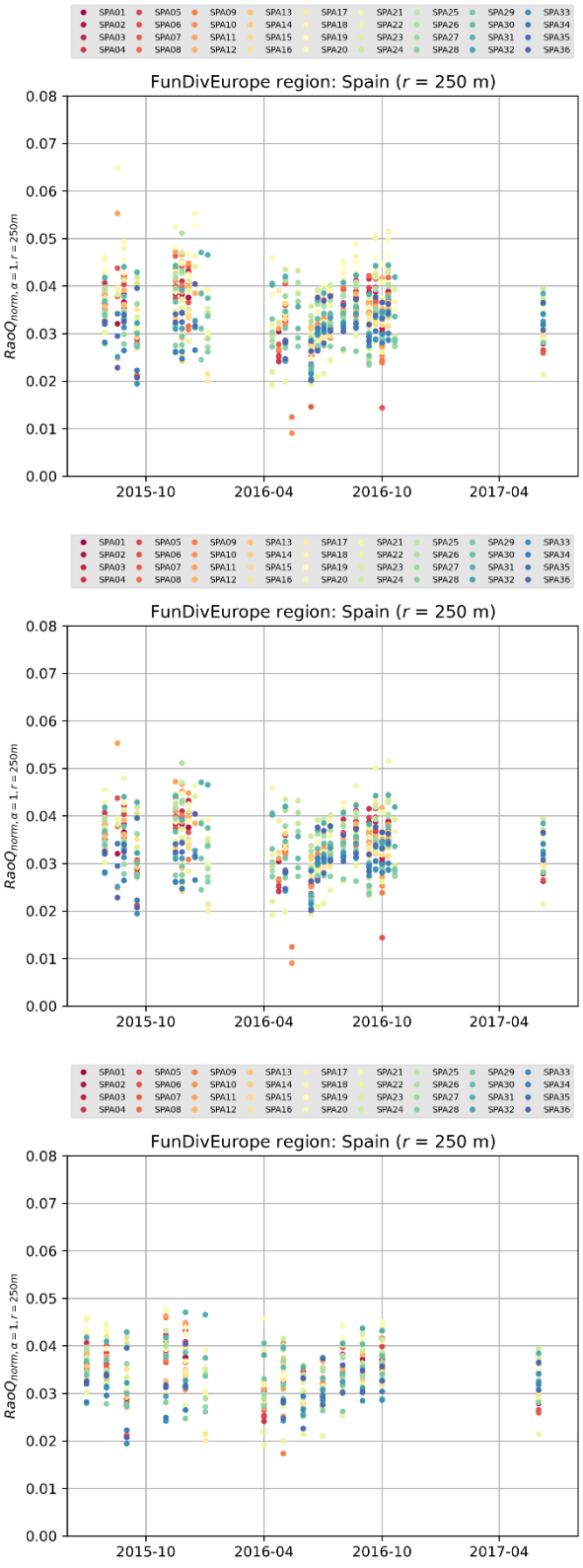

Figure 29. Average $RaoQ_{\alpha=1}$ normalized using the global approach (Pacheco-Labrador et al. under review) in circular areas of 250 m radius centered on the plots of the FunDivEUROPE network in Spain computed with no correction (top), interpolation of missing pixels (center), and monthly averages of the reflectance factors (bottom).

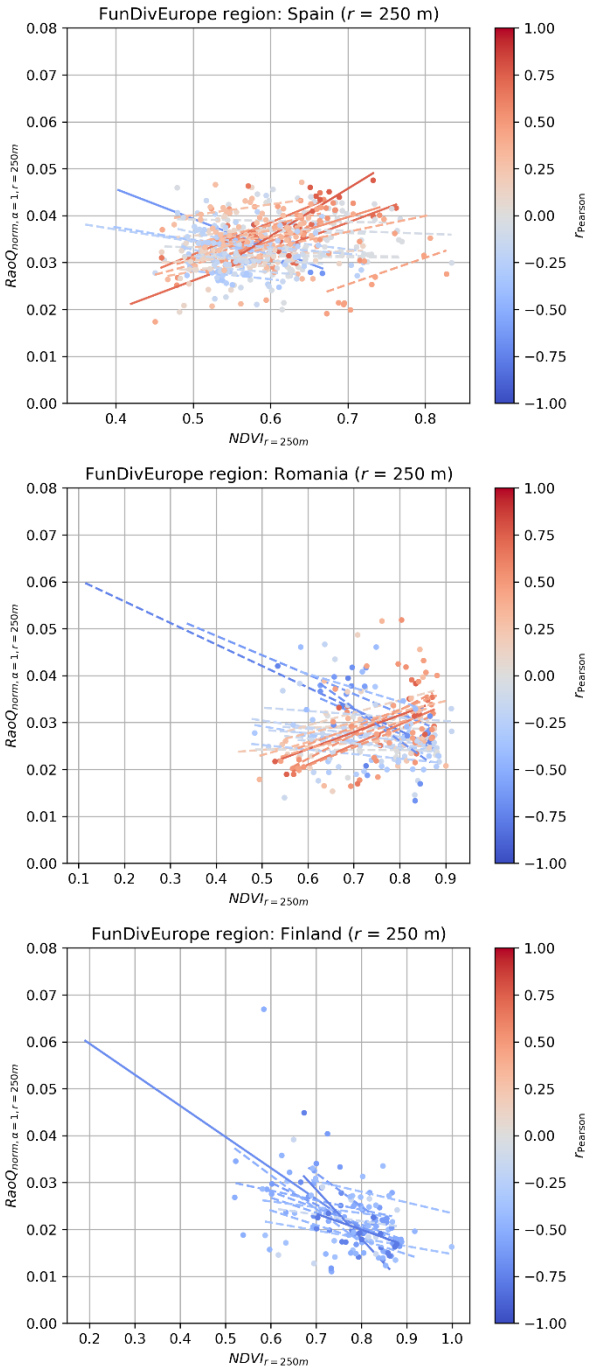

Figure 30. Average *RaoQ*$_{\alpha=1}$ normalized using the global approach (Pacheco-Labrador et al. under review) in circular areas of 250 m radius centered on the plots of the FunDivEUROPE network in Spain (top), Romania (center) and Finland (bottom). The variables are computed using monthly averages of the reflectance factors.

RD1.2 initially aimed to develop methods to predict biodiversity based on spectral, structural, and phenological information. However, the modeling work (RD1.1.1a-d) reframed the aim of this task. Sentinel-2 seemed enough to capture plant functional diversity, RADAR speckle could be problematic, and space-borne LiDAR might be limited by spectral resolution. However, the exploitation of phenological information had not been previously addressed in this context. Consequently, we focused on the phenological aspect of optical spectral diversity, addressing challenges related to the generation of time series and their interpretation. We repeated these analyses on longer time series of Sentinel-2 imagery acquired over eddy covariance towers in the context of task RD3.1. Their results matched those obtained in FunDivEUROPE. Our work has provided interesting conclusions; however, the unexpected questions arising in this process and the sometimes unclear results prevented achieving an operational processing chain. While phenology is relatively well characterized and understood, the temporal variability of plant functional diversity is yet not. This knowledge gap makes it challenging to understand which corrections improve the monitoring of plant functional diversity. Therefore, with no adequate ground information available (time series of field data), we could not confirm that the reduction in noise obtained by interpolation or averaging matched the actual state of vegetation. oBEF-Accross2 has opened essential questions and provided some hints regarding this topic, which remains to be solved in the future. In this regard, oBEF-Accross2 analyses have continued after the project thanks to a collaboration with a Ph.D. student of the Max Planck Institute for Biogeochemistry. We expect the use of newly available information, such as that provided by the network NEON can help to find robust operational processing solutions and improved interpretation.

TASK 2. MAPPING OF TD AND FD IN EUROPEAN FOREST ECOSYSTEMS USING THE METHODS DEVELOPED IN RESEARCH OBJECTIVE 1.

(Vorhersage von Biodiversität basierend auf spektraler, struktureller und phänologischer Information)

Task 2 was not fully developed during the project. Task 1 physically-based simulations provided an unprecedented understanding of the links between plant functional diversity and spectral diversity. Their conclusions revealed the potential and caveats of remote sensing in this field (RD1.1.a-d), making it not advisable to elaborate extensive maps that could not be validated with ground data. Part of the activities foreseen in Task 2 were carried out during Y2 and were expected to be concluded during Y2.5. However, small-scale Sentinel-2 analysis revealed additional challenges related to the processing of time series and the interpretation of spectral diversity through time (RD1.2). Since we could not find robust and validated solutions during Y2.5, we could not generate mature algorithms and products.

Nonetheless, Task 1 unforeseen contributions replaced the expected outputs in Task 2. These new outputs are more relevant in terms of basic scientific knowledge and applicability in an emerging field than the foreseen products. Furthermore,

cartography, processing chains, and interfaces expected in Task 2 could not have filled the fundamental knowledge gaps that Task 1 has solved. The exchange is timely, given the early stage of this emerging field, and beneficial since it has set foundational pillars for its development.

RD2.1: Development of a workflow for the processing of a large number of high-resolution satellite images for the assessment of patterns of biodiversity.

While we could not consolidate and validate an operational workflow for processing time series of remote sensing imagery, we provided valuable insight on what it should include and what challenges are yet to be solved (Figure 31). oBEF-Accross2 focused particularly on Sentinel-2 missing due to its high spatial resolution (a key factor as proven in RD1.1.b-c), and since it allowed us to deepen in the temporal domain. In addition, simulations (RD1.1.a-c) demonstrated that spectral traits' diversity is the most convenient proxy of plant functional diversity for such a multispectral mission that includes SWIR spectral bands. While we found similar performances for the spectral trait approach with different spectral configurations, SWIR bands slightly improved the robustness of the estimates (Figure 10). Therefore, as done by Ma et al. (2019), we used SWIR bands pan-sharpened from their native resolution of 20 m to the 10 m resolutions of the VNIR ones. Still, this step might not be fundamental in all cases.

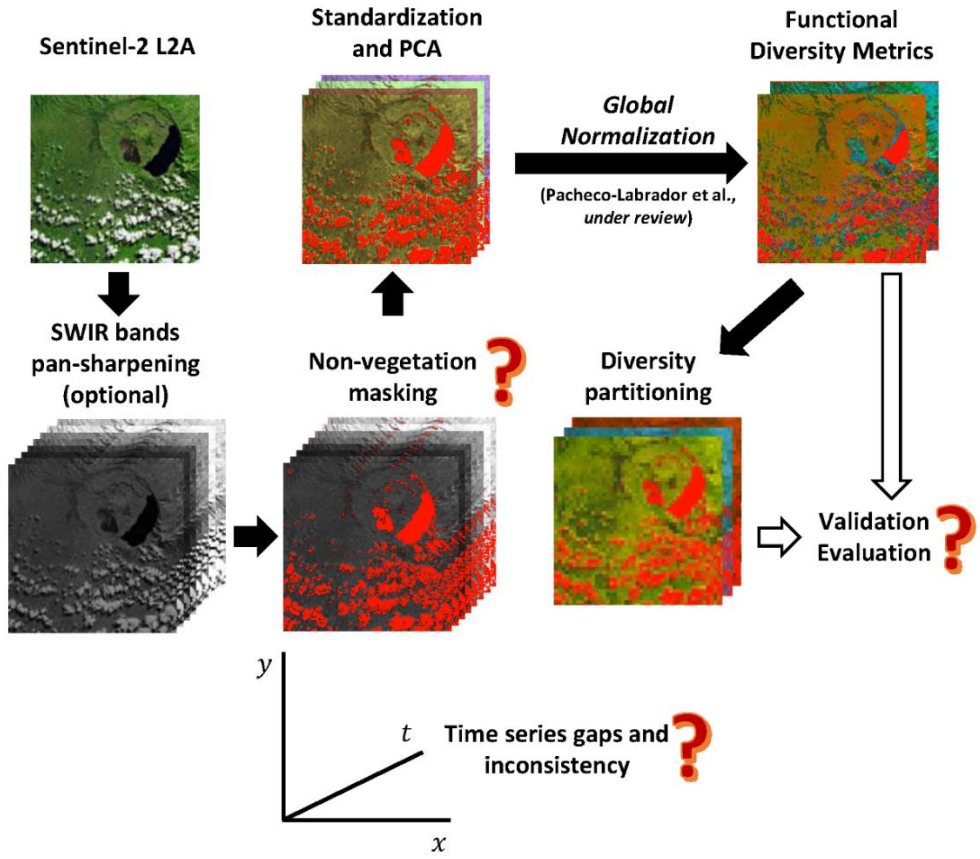

Figure 31. Flowchart of Sentinel-2 imagery processing showing the necessary and optional steps or some of the open questions identified in oBEF-Accross2. Question marks indicate questions identified and not fully solved by oBEF-Accross2.

An important decision was masking out any pixel not labeled as vegetation in the Scene Classification Layer. While this filter allows accounting for the variability of the spectral signals related to vegetation, it also sets the dilemma of modifying the sample size through time series, which affects the diversity estimates (RD1.2). We identify this as an open question regarding imagery processing for biodiversity analysis.

Our simulations also clarified that standardization and dimensionality reduction with principal component analysis must be applied to link spectral diversity with plant functional diversity during Y1 (RD1.1.b, test without these steps failed to link plant and spectral diversity metrics). It also allowed identifying the metrics that can infer plant functional diversity, such as *RaoQ*, *FDis,* and, with some considerations, *FRic*, while $RaoQ_{\alpha=1}$ provided the best estimates. Theory recommends that the former steps are applied to the entire dataset. An additional key outcome of the simulations was proving that images can be processed independently and still provide comparable FDMs. This conclusion enormously facilitates the processing of time series or global-scale imagery. In addition, during Y2.5, we developed a global normalization approach that removes the effect of dimensionality from the metrics. Global normalization makes directly comparable the *RaoQ* computed from different sensors or field datasets and improves the comparability of *FRic*. Global normalization can also be applied to diversity partitioning methods and enables the use of equivalent numbers for the first time.

oBEF-Accross2 also generated knowledge regarding the comparison of remote sensing and field estimates for validation or evaluation purposes. For example, field plots must be large enough to contain several (ideally nine at least) pixels of the sensor compared. While the plot does not need to be divided into pixel-sized subplots, it might help validate optical trait estimates, as done by Hauser et al. (2021). In addition, during the development of global normalization and the evaluation of diversity partitioning, we found that high functional or taxonomical diversity reduces the estimation accuracy of alpha diversity. This finding recommends not using very large pixel windows to analyze plant functional diversity. An additional issue that affects validation, in particular, is imagery co-registration. Pacheco-Labrador et al. (2022b) processed imagery Sentinel-2 data from two different dates and compared it with FunDivEUROPE plots' data. One of the images was georeferenced with an error of more than one pixel, which had to be corrected to match remote sensing and field estimates of plant biodiversity adequately. The influence of these errors cannot be disregarded, and automatic correction of flagging methods should be deployed.

During Y2, part of this processing chain was executed, leading to large-scale maps of FDMs computed from Sentinel-2. These images show some of the unsolved challenges identified at a small scale. Figure 32 shows some of these maps for the FunDivEUROPE regions in Spain (top), Romania (middle), and Finland (bottom). In Spain, vegetation is scattered, so bare soil occupies a large part of the scene. This leads to a spatial discontinuity of biodiversity cartography that, due to border effects and geolocation error, can complicate time series analysis. In Finland, lakes and bare soil lead as well to a patchy mapping with analysis problems similar to those in Spain.

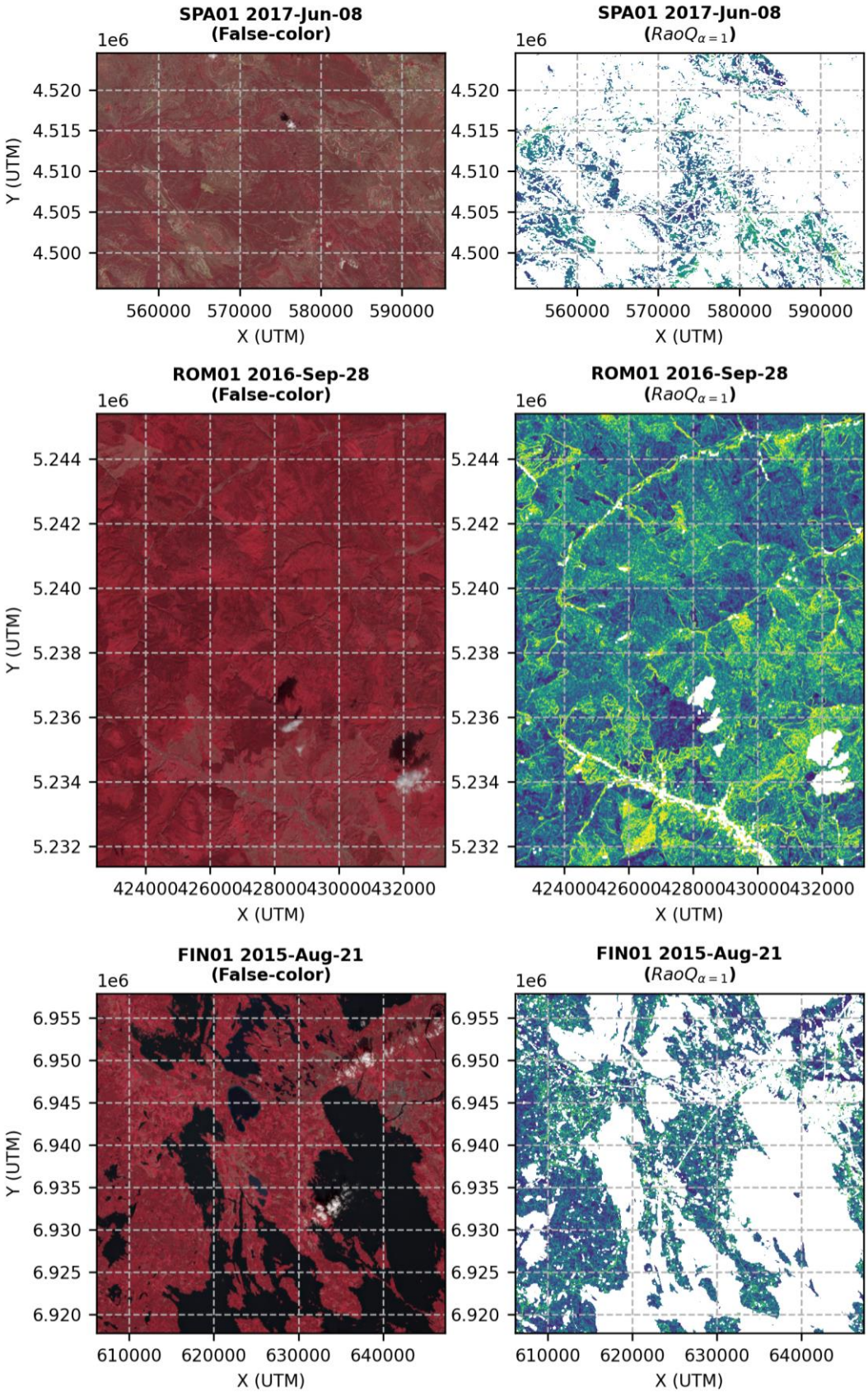

Figure 32. Sentinel-2 False-color composites (near-infrared, band 8; red; band 3; green, band 2) (left) and the corresponding Rao's Q parametric index (with α=1) map (right) for the regions covering the FunDivEUROPE plots in Spain (first row), Romania (second row) and Finland (third row).

RD2.2: Protocol for publication of the generated data products.

Open questions prevent the production of a consolidated and operational workflow as described in RD2.1. Such workflow should consider additional challenges not considered in Figure 31, such as sun and view angle variations. Still, oBEF-Accross2 has significantly contributed to the design of image analysis in the context of plant biodiversity monitoring. These recommendations are applicable to any remote sensing data. We initiated discussions regarding the use of extensive airborne hyperspectral imagery with members of FunDivEUROPE at the beginning of Y2.5, which was not foreseen initially in the project. However, the development of the global normalization approach and the problems found in the temporal domain of the analyses consumed the resources available for this opportunity.

Nonetheless, oBEF-Accross2 has consolidated different algorithms to compute functional diversity metrics from the field and remote sensing datasets and the partitioning of diversity components at different scales using a new global normalization approach. These algorithms have been gathered in the Python package *pyGNDiv* associated with a publication submitted in June 2022, and that is currently under review in Methods in Ecology and Evolution (Pacheco-Labrador et al. under review). We received positive first comments from the reviewers in November 2022. Most of the reviewer's concerns were related to the fact that the manuscript describing the modeling work (RD1.1.b-c) had not been published by the time of the submission. The remaining review process will accelerate since Pacheco-Labrador et al. (2022b) was published in July 2022. Once released in a GitHub repository when the manuscript is accepted, we *pyGNDiv* will be widely used in remote sensing of plant functional diversity and potentially in ecology studies.

RD2.3: Development of an interface between the generated biodiversity maps and the ESA ESDL.

Task 1 activities during Y1 already revealed that the spatial resolution of the ESA Earth System Data Lab (ESDL) imagery foreseen for task RD2.3 was inadequate for analyzing biodiversity-ecosystem function (BEF) relationships. Moreover, unsolving processing questions (Task 1.2) prevented the development and implementation of mature algorithms to process ESDL data. For these reasons, we decided to test the potential of remote sensing to predict plant functional diversity in the context of BEF analysis at smaller scales and in better-known environments such as stations of FunDivEUROPE, Integrated Carbon Observation System (ICOS), or FLUXNET networks. FunDivEUROPE data were collected in a previous project and had been used in Tasks 1 and 3. During Y2, we also gathered Sentinel-2 data over several ICOS stations, which were extended and increased during Y2.5 to other ICOS and FLUXNET stations. We computed functional diversity metrics from the spectral traits of this imagery using the algorithm described in Figure 31. These metrics were and are being used to assess BEF relationships in Task 3. However, since time series were gathered from different data sources (CREODIAS or GoogleEarthEngine), the processing had to be adapted to the particularities of each dataset.

TASK 3. TO ANALYSE THE IMPACT OF BIODIVERSITY ON ECOSYSTEM FUNCTIONS AND THEIR RESILIENCE.

(Analyse des Einflusses von Biodiversität auf Ökosystemfunktionen und deren Resilienz)

RD3.1: Analysis of the role of biodiversity for ecosystem functions and ecosystem services

During Y1, we collected field and remote sensing data to assess the biodiversity-ecosystem function (BEF) relationships. For example, we gathered the FunDivEUROPE field data from Prof. Xuanlong Ma (Ma et al. 2019) together with Sentinel-2 and DESIS imagery to assess the plausibility of the simulation framework (RD1.1.a-c). During Y2, we evaluated the temporal variability of Sentinel-2 spectral diversity in these sites and developed methods to deal with gaps and variability in the time series. Then, we also gathered Sentinel-2 data over ecosystem stations, such as eddy covariance towers of the ICOS network, and applied the same procedures. Moreover, we gathered ecosystem functional properties (EFPs) (Musavi et al. 2015) from (Migliavacca et al. 2021) and used Sentinel-2 data to assess the explicative role of spectral diversity on different EFPs. In addition, a Ph.D. student of the Max Planck Institute for Biogeochemistry initiated the production of field plant traits and diversity database in these sites, which was not foreseen in oBEF-Accross2. Although we originally planned some analysis of these field data in the context of oBEF-Accross2, the database production was expanded to additional sites of other networks, such as NEON, and it was not readily available by the end of the project. Still, this collaboration continued beyond oBEF-Accross2.

Eventually, we used Sentinel-2 data and EFPs to assess BEF relationships. To do so, we also considered confounding factors that could explain ecosystem functional properties (Migliavacca et al. 2021). At this stage, we tested the capability of the different temporal processing approaches developed in RD1.2 to establish the links between spectral diversity and EFPs. In addition, since EFPs summarize functional properties over long temporal periods, we also tested different ways of integrating spectral diversity in time (per image, temporal interpolation, and monthly composites). The results for per image and temporally integrated data were very similar, and only the firsts are shown (Figure 33). Finally, we selected spectral diversity (*RaoQ*) normalized with the global approach developed in RD1.1.e between the months of April and September, the growing season in the sites chosen (North hemisphere), and either computed the maximum (i.e., 95th percentile to avoid outliers) or the median $RaoQ_{norm}$.

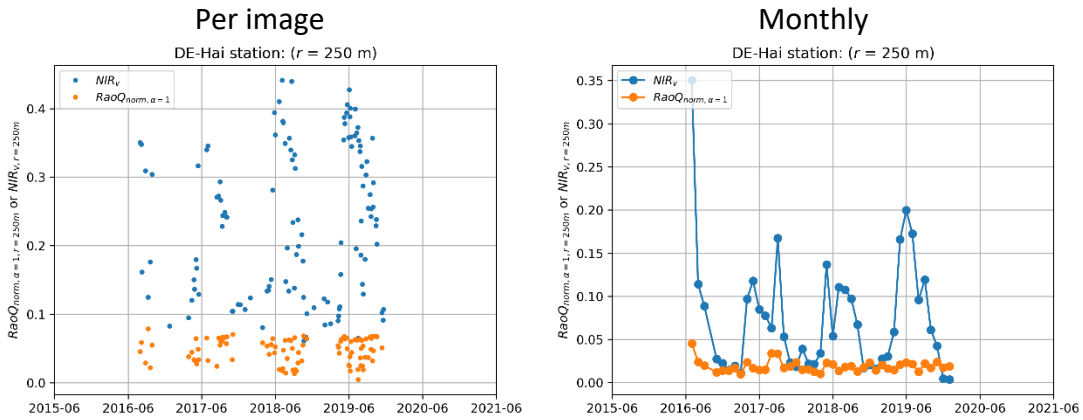

Figure 33. Time series of Sentinel-2 derived normalized difference vegetation index (*NDVI*) and Rao's quadratic entropy *Q* index with α=1 and global normalization integrated either per image (left) or from the monthly composites (right).

First, we tried to understand to what extent spectral indices such as *NDVI* integrated as $RaoQ_{norm}$ related to EFPs such as maximum leaf area index (LAI_{max}). Figure 34 compares these relationships for the per image and monthly composite *NDVI*. Unexpectedly, per-image *NDVI* shows a stronger correlation with LAI_{max} than the monthly composites. This result shows the appropriateness of the precautions taken in RD2 not to provide an operational processing chain, despite the smoother look of the monthly composites generated (e.g., Figure 33). Still, while we could expect some correlation, it is unclear whether all ecosystems should show such a correlation. Still, we could not find large differences between the maximum and median *NDVI* of the time series, which suggests that the temporal pre-processing of the time series leads to different results.

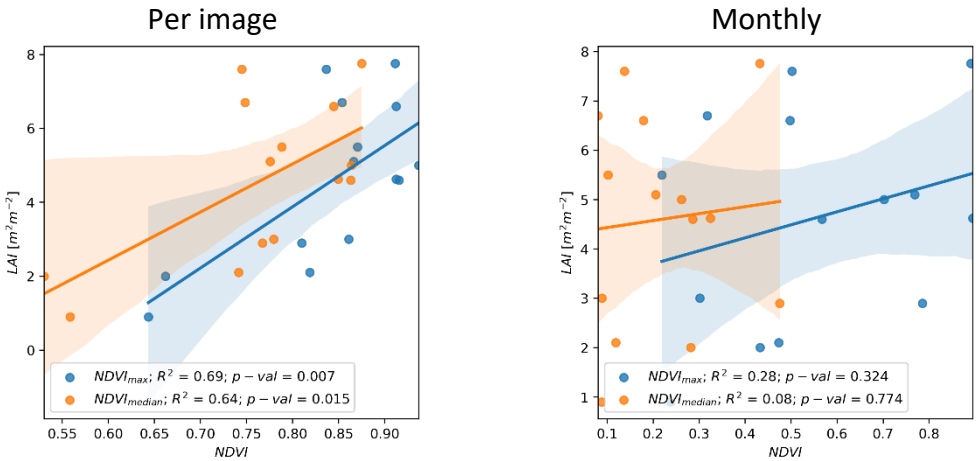

Figure 34. Correlation between LAI_{max} y *NDVI* integrated either per image (left) or from the monthly composites (right). Subplots show the maximum and the median *NDVI* computed from the images available during the growing season.

Then we used linear models to assess the explicative power of $RaoQ_{norm}$ on different EFPs. Theory suggests that while biodiversity should not be the primary driver, it could significantly contribute. Once fit over standardized metrics, we assessed the value and significance of the multilinear model coefficients where together with $RaoQ_{norm}$ the different EFPs were explained by mean incoming shortwave radiation (SW_{in}), mean air temperature (T_{air}), mean vapor pressure deficit (*VPD*), mean annual precipitation (*P*), cumulative soil water index (*CSWI*), and maximum vegetation height (H_c) derived from FLUXCOM2015, and aboveground biomass (*AGB*) derived from the Globbiomass project (Migliavacca et al. 2021).

Figure 35 presents these results. As can be seen, the main differences between the models arise from the temporal treatment. When $RaoQ_{norm}$ is computed from monthly composites (right column), there is a larger number of significant coefficients. Then $RaoQ_{norm}$ significantly explains the variability of the first principal component (*PC*1) of the EFPs, which reflects maximum ecosystem productivity. The median explains different EFPs related to productivity, such as gross primary productivity at light saturation (GPP_{sat}) and maximum basal ecosystem respiration at a reference temperature of 15 °C ($R_{b,max}$). In contrast, the maximum relates more to water-related variables (underlying water use efficiency (*uWUE*) or *WUE* based on transpiration estimates ($\underline{WUE}_t$)). Both explain the mean daytime evaporative fraction. However, we found less significant coefficients when $RaoQ_{norm}$ is computed from individual images. The median value explains the second principal component (*PC*2), which reflects ecosystem water-use strategies and, coherently, water-related variables such as *uWUE* and WUE_t, but also maximum surface conductance (GS_{max}). The maximum $RaoQ_{norm}$ did not explain any of the EFPs.

RD3.1 results require deeper analyses to be entirely conclusive. Unfortunately, the imagery was downloaded at ICOS stations before the database was selected for these analyses, which limited their match. Therefore, missing EFPs values in the database and the lack of imagery in the field stations of this dataset limited the sample size and made us exclude some important EFPs. Also, the model's fit explicative power was low in most cases. However, beyond the project, a Ph.D. student is gathering a more extensive set of remote sensing imagery and EFPs from different tower networks that will allow the continuation of these analyses. Despite these limitations, the results also open essential questions regarding how remote sensing estimates of plant functional diversity must be generated in the context of BEF relationships. While some correlations might be spurious, it might be as well the case that different processing approaches can reveal different pieces of information

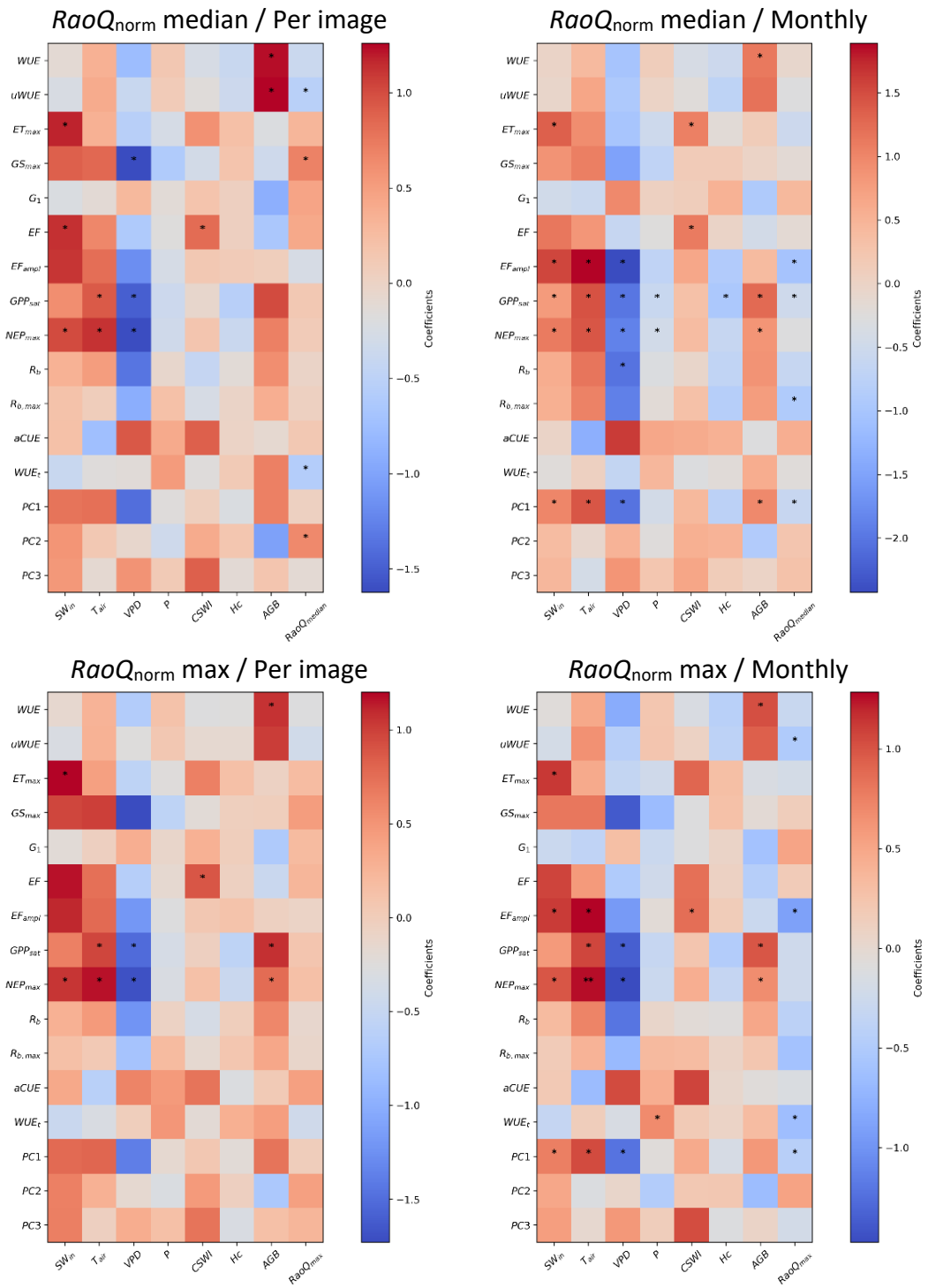

Figure 35. Standardized coefficients of the linear model between ecosystem functional properties and spectral diversity plus other confounding factors. *RaoQ*norm is computed as the median and the maximum of the growing season imagery (left; top and bottom, respectively) or the median and the maximum of the monthly composites (right; top and bottom, respectively). * -> *p*-value of the coefficient < 0.05, ** *p*-value of the coefficient < 0.001.

RD3.2: Analysis of the role of biodiversity on the stability of ecosystems

The *insurance* or *portfolio hypothesis* states that biodiversity plays a role in the stability of ecosystem responses to environmental change (e.g., García-Palacios et al., (2018)). The analyses on the role of biodiversity on stability were foreseen for the last year of the project. However, during Y1, we initiated the collection of MODIS imagery over 169 FunDivEUROPE sites and completed it in Y2. We used remote sensing and field data to compute ecosystem services indicators and functional stability metrics. Moreover, during Y2, we calculated functional diversity metrics from Sentinel-2 imagery and aggregated them at scales comparable with MODIS. In Y1, field plant functional diversity data analyzed their relationship with stability indicators.

Y1 preliminary analyses identified a weak and indirect role of plant functional diversity on ecosystem stability. This relationship was, however, controlled by mean climate and forest structure (particularly leaf area index). Y2 analyses identified that the aridity index (*AI*, the ratio of potential evaporation to precipitation) plays an essential role in ecosystem stability (Figure 36). Multivariate Adaptive Regression Splines identified *AI* as the most relevant variable, whereas plant functional diversity featured moderate importance (25%), and taxonomic diversity was found not relevant.

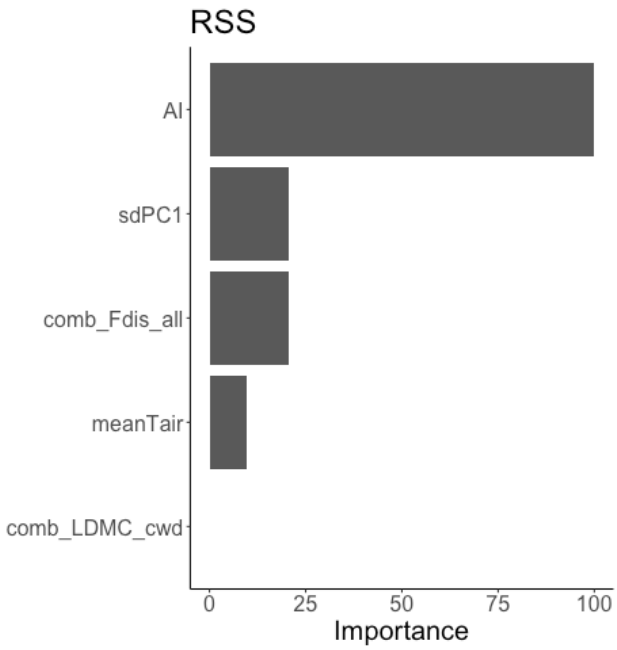

Figure 36. Feature importance of variables explaining ecosystem stability inferred from MODIS time series over FunDivEUROPE plots. Feature importance is determined using Multivariate Adaptive Regression Splines (MARS).

These results matured during Y2.5. We carried out additional analyses with structural equation modeling, which led to similar conclusions when sites with high (center) and high aridity (right) were considered together (Figure 37). Aridity plays an important role in low-aridity environments. However, the role of functional dispersion (a functional diversity metric correlated with *RaoQ*, Figure 8 and Figure 9) became relevant in high-aridity environments (right). In no case taxonomical diversity was selected as an explicative factor.

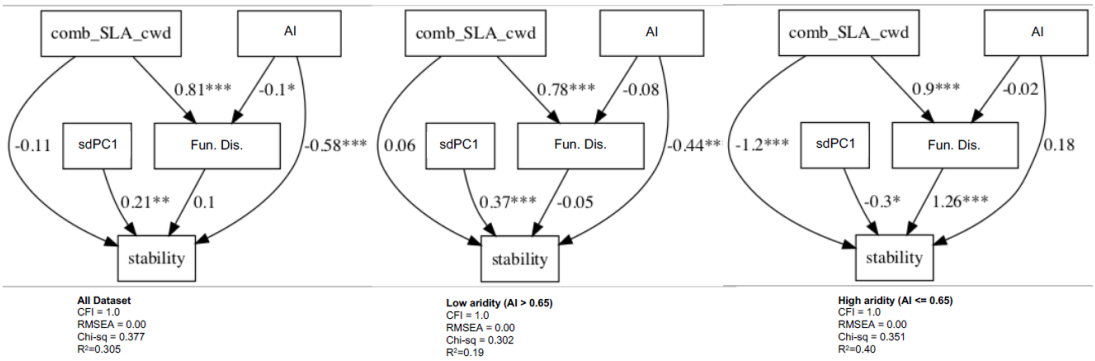

Figure 37. Results of the structural equation modeling for all sites (all dataset, left panel), low aridity (central panel), and high aridity (right panel) sites

These analyses found a marginal but significant contribution of plant functional diversity to ecosystem stability, whose relationship varied along the aridity gradient (Figure 38). Aridity increased the role of functional diversity, whereas environmental humidity (e.g., temperate and boreal forests) revealed climate as the predominant driver. These results were presented at the ICOS Science Conference held in Utrecht, Netherlands, in September 2022, whose follow-up manuscript is currently in preparation.

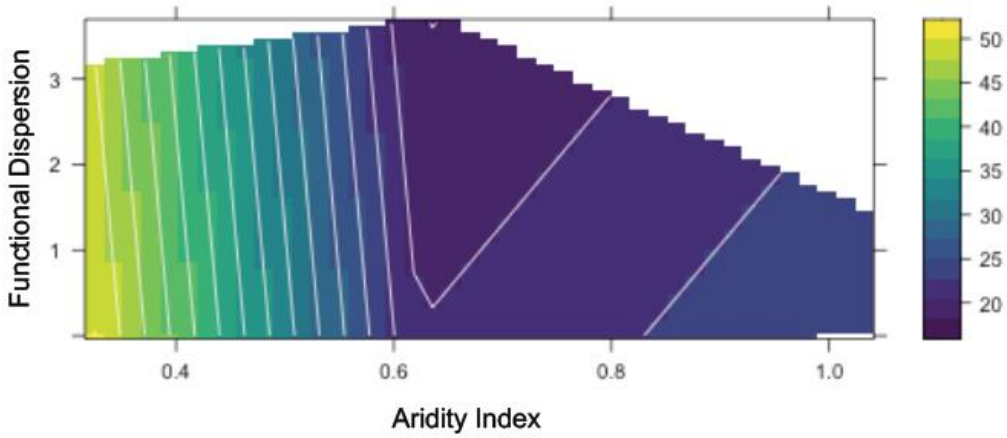

Figure 38. Mapping between aridity index and feature importance of the field estimates of plant functional diversity (characterized via functional dispersion).

REFERENCES

Baeten, L., Verheyen, K., Wirth, C., Bruelheide, H., Bussotti, F., Finér, L., Jaroszewicz, B., Selvi, F., Valladares, F., Allan, E., Ampoorter, E., Auge, H., Avăcăriei, D., Barbaro, L., Bărnoaiea, I., Bastias, C.C., Bauhus, J., Beinhoff, C., Benavides, R., Benneter, A., Berger, S., Berthold, F., Boberg, J., Bonal, D., Brüggemann, W., Carnol, M., Castagneyrol, B., Charbonnier, Y., Chećko, E., Coomes, D., Coppi, A., Dalmaris, E., Dănilă, G., Dawud, S.M., de Vries, W., De Wandeler, H., Deconchat, M., Domisch, T., Duduman, G., Fischer, M., Fotelli, M., Gessler, A., Gimeno, T.E., Granier, A., Grossiord, C., Guyot, V., Hantsch, L., Hättenschwiler, S., Hector, A., Hermy, M., Holland, V., Jactel, H., Joly, F.-X., Jucker, T., Kolb, S., Koricheva, J., Lexer, M.J., Liebergesell, M., Milligan, H., Müller, S., Muys, B., Nguyen, D., Nichiforel, L., Pollastrini, M., Proulx, R., Rabasa, S., Radoglou, K., Ratcliffe, S., Raulund-Rasmussen, K., Seiferling, I., Stenlid, J., Vesterdal, L., von Wilpert, K., Zavala, M.A., Zielinski, D., & Scherer-Lorenzen, M. (2013). A novel comparative research platform designed to determine the functional significance of tree species diversity in European forests. *Perspectives in Plant Ecology, Evolution and Systematics, 15*, 281-291

Benavides, R., Scherer-Lorenzen, M., & Valladares, F. (2019a). The functional trait space of tree species is influenced by the species richness of the canopy and the type of forest. *Oikos, 128*, 1435-1445

Benavides, R., Valladares, F., Wirth, C., Müller, S., & Scherer-Lorenzen, M. (2019b). Intraspecific trait variability of trees is related to canopy species richness in European forests. *Perspectives in Plant Ecology, Evolution and Systematics, 36*, 24-32

Botta-Dukát, Z. (2005). Rao's quadratic entropy as a measure of functional diversity based on multiple traits. *Journal of Vegetation Science, 16*, 533-540

de Bello, F., Lavergne, S., Meynard, C.N., Lepš, J., & Thuiller, W. (2010). The partitioning of diversity: showing Theseus a way out of the labyrinth. *Journal of Vegetation Science, 21*, 992-1000

Fassnacht, F.E., Müllerová, J., Conti, L., Malavasi, M., & Schmidtlein, S. (2022). About the link between biodiversity and spectral variation. *Applied Vegetation Science, 25*, e12643

Feret, J.-B., François, C., Asner, G.P., Gitelson, A.A., Martin, R.E., Bidel, L.P.R., Ustin, S.L., le Maire, G., & Jacquemoud, S. (2008). PROSPECT-4 and 5: Advances in the leaf optical properties model separating photosynthetic pigments. *Remote Sensing of Environment, 112*, 3030-3043

García-Palacios, P., Gross, N., Gaitán, J., & Maestre, F.T. (2018). Climate mediates the biodiversity–ecosystem stability relationship globally. *Proceedings of the National Academy of Sciences, 115*, 8400

Gómez-Dans, J.L., Lewis, P.E., & Disney, M. (2016). Efficient Emulation of Radiative Transfer Codes Using Gaussian Processes and Application to Land Surface Parameter Inferences. *Remote Sensing, 8*, 119

Hauser, L.T., Féret, J.-B., An Binh, N., van der Windt, N., Sil, Â.F., Timmermans, J., Soudzilovskaia, N.A., & van Bodegom, P.M. (2021). Towards scalable estimation of plant functional diversity from Sentinel-2: In-situ validation in a heterogeneous (semi-)natural landscape. *Remote Sensing of Environment, 262*, 112505

Hosgood, B., Jacquemoud, S., Andreoli, G., Verdebout, J., Pedrini, G., & Schmuck, G. (1994). Leaf Optical Properties EXperiment 93 (LOPEX93). In E.C.J.R. Centre (Ed.). Ispra (Italy). Available online: [http://opticleaf.ipgp.fr/databases/LDB_lopex1993.xls], last accessed 11-Nov-2020

Jacquemoud, S., Verhoef, W., Baret, F., Bacour, C., Zarco-Tejada, P.J., Asner, G.P., François, C., & Ustin, S.L. (2009). PROSPECT+SAIL models: A review of use for vegetation characterization. *Remote Sensing of Environment, 113*, S56-S66

Jost, L. (2006). Entropy and diversity. *Oikos, 113*, 363-375

Jost, L. (2007). PARTITIONING DIVERSITY INTO INDEPENDENT ALPHA AND BETA COMPONENTS. *Ecology, 88*, 2427-2439

Laliberté, E., & Legendre, P. (2010). A distance-based framework for measuring functional diversity from multiple traits. *Ecology, 91*, 299-305

Laliberté, E., Schweiger, A.K., & Legendre, P. (2020). Partitioning plant spectral diversity into alpha and beta components. *Ecology Letters, 23*, 370-380

Ma, X., Mahecha, M.D., Migliavacca, M., van der Plas, F., Benavides, R., Ratcliffe, S., Kattge, J., Richter, R., Musavi, T., Baeten, L., Barnoaiea, I., Bohn, F.J., Bouriaud, O., Bussotti, F., Coppi, A., Domisch, T., Huth, A., Jaroszewicz, B., Joswig, J., Pabon-Moreno, D.E., Papale, D., Selvi, F., Laurin, G.V., Valladares, F., Reichstein, M., & Wirth, C. (2019). Inferring plant functional diversity from space: the potential of Sentinel-2. *Remote Sensing of Environment, 233*, 111368

Mason, N.W.H., Mouillot, D., Lee, W.G., & Wilson, J.B. (2005). Functional richness, functional evenness and functional divergence: the primary components of functional diversity. *Oikos, 111*, 112-118

Migliavacca, M., Musavi, T., Mahecha, M.D., Nelson, J.A., Knauer, J., Baldocchi, D.D., Perez-Priego, O., Christiansen, R., Peters, J., Anderson, K., Bahn, M., Black, T.A., Blanken, P.D., Bonal, D., Buchmann, N., Caldararu, S., Carrara, A., Carvalhais, N., Cescatti, A., Chen, J., Cleverly, J., Cremonese, E., Desai, A.R., El-Madany, T.S., Farella, M.M., Fernández-Martínez, M., Filippa, G., Forkel, M., Galvagno, M., Gomarasca, U., Gough, C.M., Göckede, M., Ibrom, A., Ikawa, H., Janssens, I.A., Jung, M., Kattge, J., Keenan, T.F., Knohl, A., Kobayashi, H., Kraemer, G., Law, B.E., Liddell, M.J., Ma, X., Mammarella, I., Martini, D., Macfarlane, C., Matteucci, G., Montagnani, L., Pabon-Moreno, D.E., Panigada, C., Papale, D., Pendall, E., Penuelas, J., Phillips, R.P., Reich, P.B., Rossini, M., Rotenberg, E., Scott, R.L., Stahl, C., Weber, U., Wohlfahrt, G., Wolf, S., Wright, I.J., Yakir, D., Zaehle, S., & Reichstein, M. (2021). The three major axes of terrestrial ecosystem function. *Nature, 598*, 468-472

Musavi, T., Mahecha, M.D., Migliavacca, M., Reichstein, M., van de Weg, M.J., van Bodegom, P.M., Bahn, M., Wirth, C., Reich, P.B., Schrodt, F., & Kattge, J. (2015). The imprint of plants on ecosystem functioning: A data-driven approach. *International Journal of Applied Earth Observation and Geoinformation, 43*, 119-131

North, P.R.J. (1996). Three-dimensional forest light interaction model using a Monte Carlo method. *IEEE Transactions on Geoscience and Remote Sensing, 34*, 946-956

Pacheco-Labrador, J., de Bello, F., Migliavacca , M., Ma, X., Carvalhais, N., & Wirth, C. (under review). Global normalization of plant functional diversity metrics for remote sensing. *Methods in Ecology and Evolution*

Pacheco-Labrador, J., El-Madany, T.S., Martin, M.P., Gonzalez-Cascon, R., Carrara, A., Moreno, G., Perez-Priego, O., Hammer, T., Moossen, H., Henkel, K., Kolle, O.,

Martini, D., Burchard, V., van der Tol, C., Segl, K., Reichstein, M., & Migliavacca, M. (2020a). Combining hyperspectral remote sensing and eddy covariance data streams for estimation of vegetation functional traits. *Biogeosciences Discuss., 2020*, 1-38

Pacheco-Labrador, J., El-Madany, T.S., van der Tol, C., Martin, M.P., Gonzalez-Cascon, R., Perez-Priego, O., Guan, J., Moreno, G., Carrara, A., Reichstein, M., & Migliavacca, M. (2021). senSCOPE: Modeling mixed canopies combining green and brown senesced leaves. Evaluation in a Mediterranean Grassland. *Remote Sensing of Environment, 257*, 112352

Pacheco-Labrador, J., El-Madany, T.S., van der Tol, C., Martín, M.P., Gonzalez-Cascon, R., Perez-Priego, O., Guan, J., Moreno, G., Carrara, A., Reichstein, M., & Migliavacca, M. (2020b). senSCOPE: Modeling radiative transfer and biochemical processes in mixed canopies combining green and senescent leaves with SCOPE. *bioRxiv*, 2020.2002.2005.935064

Pacheco-Labrador, J., Migliavacca, M., Ma, X., Machecha, M., Carvalhais, N., Weber, U., Benavides, R., Bouriaud, O., Barnoaiea, I., Coomes, D.A., Bohn, F.J., Kraemer, G., Heiden, U., Huth, A., & Wirth, C. (2022a). Strengths and limitations in remote sensing of plant functional diversity. Drawing the lines with radiative transfer modeling and satellite observations. In ESA (Ed.), *ESA Living Planet Symposium 2022*. Bohn, Germany. 23-27 May 2022. (Oral Communication)

Pacheco-Labrador, J., Migliavacca, M., Ma, X., Mahecha, M.D., Carvalhais, N., Weber, U., Benavides, R., Bouriaud, O., Barnoaiea, I., Coomes, D.A., Bohn, F.J., Kraemer, G., Heiden, U., Huth, A., & Wirth, C. (2022b). Challenging the link between functional and spectral diversity with radiative transfer modeling and data. *Remote Sensing of Environment, 280*, 113170

Pacheco-Labrador, J., Weber, U., Ma, X., Mahecha, M.D., Carvalhais, N., Wirth, C., Huth, A., Bohn, F.J., Kraemer, G., Heiden, U., FunDiv, E.m., & Migliavacca, M. (2022c). Evaluating the potential of DESIS to infer plant taxonomical and functional diversities in European forests. *Int. Arch. Photogramm. Remote Sens. Spatial Inf. Sci., XLVI-1/W1-2021*, 49-55

Rocchini, D., Marcantonio, M., Da Re, D., Bacaro, G., Feoli, E., Foody, G.M., Furrer, R., Harrigan, R.J., Kleijn, D., Iannacito, M., Lenoir, J., Lin, M., Malavasi, M., Marchetto, E., Meyer, R.S., Moudry, V., Schneider, F.D., Šímová, P., Thornhill, A.H., Thouverai, E., Vicario, S., Wayne, R.K., & Ricotta, C. (2021). From zero to infinity: Minimum to maximum diversity of the planet by spatio-parametric Rao's quadratic entropy. *Global Ecology and Biogeography, 30*, 1153-1162

Schneider, F.D., Morsdorf, F., Schmid, B., Petchey, O.L., Hueni, A., Schimel, D.S., & Schaepman, M.E. (2017). Mapping functional diversity from remotely sensed morphological and physiological forest traits. *Nature Communications, 8*, 1441

Skidmore, A.K., Coops, N.C., Neinavaz, E., Ali, A., Schaepman, M.E., Paganini, M., Kissling, W.D., Vihervaara, P., Darvishzadeh, R., Feilhauer, H., Fernandez, M., Fernández, N., Gorelick, N., Geijzendorffer, I., Heiden, U., Heurich, M., Hobern, D., Holzwarth, S., Muller-Karger, F.E., Van De Kerchove, R., Lausch, A., Leitão, P.J., Lock, M.C., Mücher, C.A., O'Connor, B., Rocchini, D., Roeoesli, C., Turner, W., Vis, J.K., Wang, T., Wegmann, M., & Wingate, V. (2021). Priority list of biodiversity metrics to observe from space. *Nature Ecology & Evolution, 5*, 896-906

Tagliabue, G., Pacheco-Labrador, J., Panigada, C., Carrara, A., Cascón, R.G., Colombo, R., El-Madany, T., Martín, M.P., Marcos, G.M., Rascher, U., Rolo, V., Migliavacca, M., & Rossini, M. (2022). Unravelling the functional diversity of a dehesa with sun-induced fluorescence. In, *World Biodiversity Forum 2022* Davos, Switzerland, June 26 - July 1, 2022

van der Tol, C., Verhoef, W., Timmermans, J., Verhoef, A., & Su, Z. (2009). An integrated model of soil-canopy spectral radiances, photosynthesis, fluorescence, temperature and energy balance. *Biogeosciences, 6*, 3109-3129

Wang, R., & Gamon, J.A. (2019). Remote sensing of terrestrial plant biodiversity. *Remote Sensing of Environment, 231*, 111218